Advances on surface structural determination by LEED



2011 J. Phys.: Condens. Matter 23 303001

(http://iopscience.iop.org/0953-8984/23/30/303001)

IOP Publishing Journal of Physics: Condensed Matter

J. Phys.: Condens. Matter **23** (2011) 303001 (19pp) doi:10.1088/0953-8984/23/30/303001

TOPICAL REVIEW

# Advances on surface structural determination by LEED

**Edmar A Soares[1,3], Caio M C de Castilho[2] and Vagner E de Carvalho[1]**

[1] Departamento de Física, ICEX, Universidade Federal de Minas Gerais, 31270-090, Belo Horizonte, MG, Brazil

[2] Grupo de Física de Superfícies e Materiais, Instituto de Física and Instituto Nacional de Ciência e Tecnologia em Energia e Ambiente (CIENAM)INCT-E&A, Universidade Federal da Bahia, Campus Universitário da Federação, 40170-115, Salvador, BA, Brazil

E-mail: edmar@fisica.ufmg.br

Received 22 July 2010, in final form 12 May 2011
Published 12 July 2011
Online at stacks.iop.org/JPhysCM/23/303001

**Abstract**

In the last 40 years, low energy electron diffraction (LEED) has proved to be the most reliable quantitative technique for surface structural determination. In this review, recent developments related to the theory that gives support to LEED structural determination are discussed under a critical analysis of the main theoretical approximation—the muffin-tin calculation. The search methodologies aimed at identifying the best matches between theoretical and experimental intensity versus voltage curves are also considered, with the most recent procedures being reviewed in detail.

(Some figures in this article are in colour only in the electronic version)

## Contents



[3] Author to whom any correspondence should be addressed.

## 1. Introduction

The experimental use of electrons as a tool for probing surfaces can be traced back to the time around the first quarter of the 20th century when the wave character of electrons was, for the first time, experimentally demonstrated. Preliminary works by de Broglie, with respect to the wave nature of particles, led Elsasser [1] to interpret the results by Davisson and Kunsman [2] as somehow related to the crystal structure. A more complete account of this possibility of electrons giving information about crystal surfaces was provided by Davisson and Germer in 1927 [3, 4]. The potential impact of electron diffraction on surface structural determination is illustrated by the fact that Wood [5], when presenting a seminal paper about the nomenclature of surface crystallography, mentions the activity in low energy electron diffraction (LEED; then called slow electron diffraction) as an important reason for such nomenclature.

Despite this early evidence of electron diffraction as a phenomenon that could be applied to surface structural determination, its use as a routine tool was partially prevented

 

by the requirement of keeping the surface under study uncontaminated (or contaminated in a controllable manner) during the experiment. The experimental time interval is in the range of hours, during which the pressure around the sample must be kept at least at $10^{-10}$ Torr (1 Torr = 1 mm Hg = 133.322 Pa). This became possible only after the development of ultra-high-vacuum (UHV) techniques in the 1960s. Another aspect that contributed to the delay in an effective application of LEED to surface studies was the lack of a theoretical approach to deal with the strong interaction of electrons with surface atoms. The large cross section of electron–atom scattering, mainly due to particle charge, results in an interaction that is much more complex than in x-rays, requiring a dynamic (multiple scattering) treatment. Besides, the computer codes and equipment presently used in calculations were not available before the middle of the 20th century. Since then, LEED has been responsible for the structural determination of most solved surfaces [6–8].

Traditional crystallographic methods, using x-ray scattering, give information about the bulk structure. This results from the fact that, as each atomic plane scatters just a small portion of the incident radiation, the collectible scattered beams essentially come from internal planes of the crystal. The strong electron–atom interaction in the case of LEED results in a small penetration depth for the incident beam, with each atomic plane scattering a significant portion of the incident beam, so that information carried out by the scattered electrons essentially describes the first few layers of the sample.

The low energy electrons used as a probe in LEED have a complex interaction with the first few layers of atoms, a phenomenon called the multiple scattering process [9–11], where the incident electrons are elastically scattered more than once. This multiple scattering process occurs not only in the scattering of electrons by the atoms within the layers, but also between different layers. Due to the complexity of this scattering process, as compared with x-ray diffraction, the LEED technique presents a significant theoretical disadvantage: the impossibility (or at least a difficulty) of directly 'inverting' experimental data using, for example, an approach similar to the Patterson function method [12].

The structural determination of a surface via LEED is a process with two stages. First, after preparing the sample and placing it in appropriate experimental conditions, the scattered beam intensities are collected and numerically treated as a function of energy of the incident beam, in different directions. These curves are usually called LEED-IV curves, since the incident electron energy is a function of the voltage applied to the electron gun. Second, one must formulate models for the surface and perform a theoretical calculation of the scattered intensity as a function of voltage, assuming the existence of long-range order on the surface. This is then followed by a quantitative comparison of the two sets of curves, experimental and theoretical. To perform the calculations, it is necessary to assume values for a set of structural and non-structural parameters, each significantly affecting the calculation output. An eventual coincidence between theoretical and experimental curves supports the belief that the set of parameters used in the theory corresponds to the actual surface. Thus, structural determination involves a search process of an adequate set of parameters for which the degree of coincidence between the two sets of curves is maximized.

As described above, LEED structural determination requires a calculation process in order to computationally mimic the structure of the real surface. A model for the surface structure, having as an initial guess the bulk structure and other information of experimental or theoretical nature, is conceived and a set of theoretically calculated LEED-IV curves are computed. To do this, it is necessary to assume sensible values for a large number of structural and non-structural parameters, namely inter-planar distances, atomic coordinates within the unit cell, phase shifts associated to the scattering potential, parameters related to thermal effects like the Debye temperature for bulk and surface layers, the muffin-tin zero potential, etc. Therefore, the structural determination of surfaces using LEED essentially becomes a search problem. The surface determination is ideally achieved when it becomes possible to fit, up to an acceptable degree, the two sets of curves, experimental and theoretical. These curves are compared to each other using a reliability factor ($R$ factor) which constitutes a quantitative measure of the degree of agreement between them [9]. There are several definitions for the $R$ factor but what matters the most is that it represents the best fitting between the curves. A perfect fitting is, in fact, impossible, as a result of experimental errors and the not-so-perfect adequacy of the proposed theoretical model. It is important to be aware that any theoretical model involves approximations, to a higher or a lower degree. For carefully obtained experimental curves, the search for the best agreement between the two sets of LEED-IV curves is theoretically done in two ways: (a) by perfecting and improving the theoretical model that gives support to the calculations and (b) by varying the structural and non-structural parameters for the adopted theoretical model in a more efficient way. In the second case, as the number of possible structures is large and the theoretical curves are strongly dependent on the parameter values, it is essential to establish a route for varying these parameters. The $R$-factor values at each point in the parameter space form a hypersurface with several maxima and minima. In the search process the structural determination is achieved when it is possible to identify the global minimum among the several minima for the $R$ factor. The $R$ factor is then a cost function that must be minimized. Despite being necessary to establish a route for determining a global minimum [13], a critical problem of the search is how to be sure that a global minimum has been achieved as opposed to simply a local minimum.

In the last 15 years, higher quality datasets were made possible by technical advances such as (a) the use of channel plates as a detector for the diffracted beams instead of the standard phosphor screen [6, 14, 15] and (b) the development of low current electron guns that allowed the design of LEED optics for applications on sensitive samples where nanoampere or picoampere levels are required [16–19]. Despite these technical advances, the technique still uses basically the same procedures that were used when a computer-controlled acquisition process was adopted [20, 21]. On the other hand,

more advances have been observed in the analysis of the experimental datasets. Therefore, in this review, we focus on recent contributions to the theoretical aspects of LEED structural determination.

This paper is organized as follows. In section 2, theoretical approaches to the problem are discussed including approaches for a better description of the scattering potential, the extension of the LEED technique to single nanostructures, the tensor LEED approximation and the use of direct methods to recover structural information from the LEED pattern. In section 3 advances in the search process for maximizing the coincidence between theoretical and experimental LEED-IV curves are presented. Section 4 contains the conclusions and perspectives.

## 2. Theoretical aspects

### *2.1. The electron scattering potential*

In the surface structure determination by LEED, the interaction of the incident electrons with the crystal constituents has to be described through a multiple scattering process and, thus, the crystal potential has to be theoretically modeled. In fact, nearly all previous LEED calculations have been performed by employing an average potential, using a 'muffin-tin' (MT) shape [22, 23] for the expansion of the wavefunctions in order to describe the multiple scattering process. In this approximation, the potential is averaged around the ionic core within a chosen radius ($r_{\mathrm{MT}}$) and assumed constant in the interstitial region between the atoms as shown in figure 1. The assumption of a constant inter-atomic potential is certainly a drastic approximation, particularly when the electron kinetic energy is close to the value of the constant potential. However, although this theoretical approximation has been generally used in solid state physics and surface physics, and has shown good results for several materials like metals, it does not work so well for materials with covalent bonds, where the potential is known to be much less isotropic. This inadequacy also occurs for some classes of metal oxides, where effects of charge transfer between oxygen and metal atoms must be taken into account.

In order to obtain the theoretical LEED-IV curves, an MT potential is considered for the process of electronic scattering from individual atoms in the surface region and these calculations yield the phase shifts for the scattering process. As the phase shifts are the quantities that determine the conditions for the diffraction process, the potential used in the calculation is very important for the accuracy of the structural determination. For typically covalent materials, like semiconductors, the LEED analysis always shows a poorer theory–experiment agreement (higher $R$ factor) when compared to the values obtained for metals. In fact, the choice of the 'right' MT radii for the atoms is very difficult and, usually, they have been arbitrarily adjusted in order to reach a good theory–experiment agreement.

Ideally, the phase shifts should be evaluated employing a full potential calculation. In fact, there are a number of different approaches that have been proposed for bulk electronic structures [24–27]. However, these approaches have not yet been applied to surfaces, mainly as a result of the amount of computer time required.

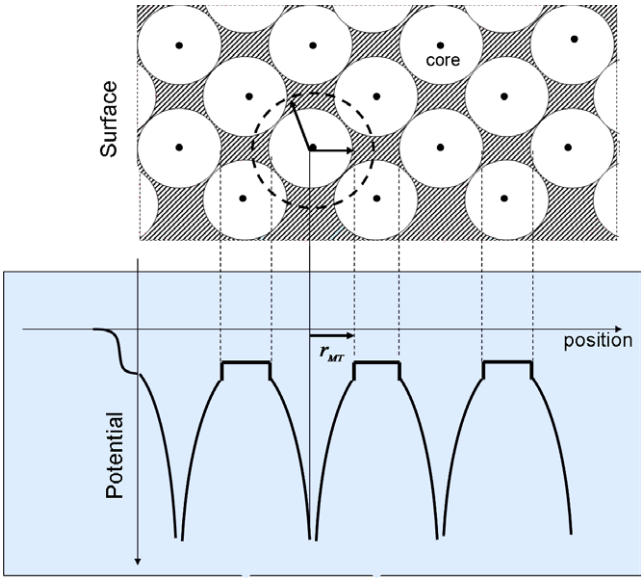


**Figure 1.** Schematic representation of the MT approximation used in LEED to evaluate the scattering phase shifts.

Hence, no great advance in the phase shift calculations for low energy electron scattering has been verified in the last decade except for two approaches that seem to be useful in LEED analysis, namely the optimized MT potential and the multi-slice finite difference method. The optimized MT potential proposed by Rundgren [28] allows a better estimation of the MT radii, while the multi-slice finite difference method for the full potential calculation, as proposed by Wu *et al* [29], seems to be a promising procedure for theoretically obtaining the low energy electron diffraction spectra.

*2.1.1. The optimized muffin-tin potential.* To improve the scattering potential used to calculate the electron phase shifts, Rundgren [28] suggested a procedure for elastic electron scattering in a surface slab that searches for the best radius of the MT sphere which minimizes the potential discontinuity between the spherical and interstitial regions. These discontinuities may produce standing electron waves in the MT atoms, generating undesirable scattering resonances [30]. Thus, resonance features in phase shifts and differential scattering cross sections are almost eliminated. Although this effect is more pronounced in the low energy range, it has been shown that such corrections may reduce the reliability factor, leading to a more precise structural determination [30].

In the conventional MT potential calculations, electronic densities are obtained from the contributions of neutral atoms, usually from atomic self-consistent relativistic calculations. The total potential for an electron moving elastically, with energy $E$ through the surface slab, is obtained from a superposition of free-atom potentials. This procedure generates spherical potential wells for the atoms of the surface slab ($V_{\mathrm{sph}}(r)$), associated with the Madelung potential ($V_{\mathrm{M}}(r)$), this due to nonzero valence. There is also the measured

surface core level shifts ($V_{CL}$) and the inherent exchange–correlation potential ($V_{xc}(E, r)$) of the free atoms modeled by a local density functional. With the aim of taking into account the surface core level shifts, Rundgren proposed a different approach, which resulted in the methodology presented below [28, 31].

The total potential can be written as

$$V_T(E, r) = V_{sph}(r) + V_M(r) + V_{CL} + V_{xc}(E, r). \quad (1)$$

A crystal atom $i$ is modeled as a charged sphere of radius $R_i$ defined by the condition that the electron density $\rho_i(r)$, for $r < R_i$, matches the nuclear charge $Z_i$ and valence $\nu_i$, so that

$$\int_0^{R_i} 4\pi\rho_i(r)r^2\,dr = Z_i + \nu_i. \quad (2)$$

The MT spheres of potential $V_T(E, r)$ are assumed to be centered onto the atomic lattice points, without overlapping but touching each other at a point along the line between the nuclei, with radii $r_{(MT)i}$ (in proportions determined by the atomic species). In principle, such radii are constant with respect to energy. The potential in the region between the spheres is also assumed constant. This model shows a potential discontinuity at the MT radii and, for the electron scattering process, these steps are responsible for resonance effects in the phase shifts. However, the definition of the MT radii for each system, as well as the value of the potential at the MT radius [32], is not straightforward.

According to Loucks's prescription [23], the interstitial potential of a surface slab with $N$ atoms is

$$V_0(E) = \sum_{i=1}^{N} w_i \int_i^{R_i} 4\pi V_{xc}(E, r)r^2\,dr \quad (3)$$

where $w_i$ is a renormalization factor and $r_i$ is the radius of shells surrounding the MT spheres. At the MT radii, $r_{(MT)i}$, the crystal potential has steps of height

$$s_i(E) = V_T(E, r_i) - V_0(E, r_1, r_2, \ldots, r_N) \quad (4)$$

for $r \leqslant r_{opt(i)}$, where $r_{opt(i)}$ is the radius corresponding to the optimum value. By imposing the minimization condition for the quantity

$$\sum_{i=1}^{N} w_i \left[ s_i(E) - \sum_{j=1}^{N} w_j s_j(E) \right]^2 \quad (5)$$

the potential steps $s_i(E)$ approach the step average as the $r_{(MT)i}$ radii are successively adjusted and their optimum values ($r_{opt(i)}$) give rise to a common (averaged) potential step $s_{ave}(E)$ at all MT radii. In fact, the best radius is the one which minimizes the potential jump between the sphere and the interstitial region. Thus, a continuous potential can be obtained by

$$V_T^{opt}(E, r) = V_T(E, r) - s_{ave}(E); \qquad (r \leqslant r_{opt}(i)). \quad (6)$$

This kind of potential is supposed to overcome difficulties like defining an MT radii appropriate for the crystal under study and to avoid resonance effects due to discontinuities in the potential. Also, the inclusion of an energy-dependent interstitial potential, related to the real part of the inner potential ($V_{0r}$), as defined in LEED, is allowed in a natural way. In the usual LEED energy range, the $V_{0r}$ versus $E$ curve can be well approximated by an analytical expression with three adjustable parameters $c_0$, $c_1$ and $c_2$ [33], given by

$$V_{0r}(E) = E - V_{0r}^{const} + c_0 + \frac{c_1}{\sqrt{E + c_2}} \quad (7)$$

where the fit is a three-dimensional nonlinear minimization problem. These parameters are adjusted according to the specific sample composition (see, for example, [30, 34, 35]).

This optimized MT potential approach has proved to be suitable for the calculations of the LEED-IV curves for metal oxides and alloys. For example, Nascimento *et al* [30] have used this approach in a structural LEED analysis of the (001) surface of the metal oxide $Ca_{1.5}Sr_{0.5}RuO_4$ and concluded that an acceptable final theory–experiment agreement was obtained when the optimized MT radii phase shifts were used. This method has also been applied in the studies of the $Fe_3O_4(100)$ surface [36, 37], clean surfaces of $\alpha$-$Fe_2O_3(0001)$, to $\alpha$-$Cr_2O_3(0001)$ bulk single crystals [38] and also for the partial dissociation of water on $Fe_3O_4(100)$ [39], where it has been observed that it leads to reliable results. Derry *et al* [40] have also used, with success, the optimized MT potential procedure for the study of the structure and composition of the NiPd(110) surface. On the other hand, Meyer *et al* [41], in a study of the surface structure of polar $Co_3O_4(111)$ films grown epitaxially on Ir(100)-(1 × 1), compared the final theory–experiment agreement, using phase shifts calculated by the optimized MT potential (ionic crystal), with those from the neutral-atom calculation on a rocksalt-type CoO and observed that the use of the latter resulted in a better $R$-factor value. Also, in a structural determination of Pd(100)($\sqrt{5}\times\sqrt{5}$)-R27°–O surface oxide, Kostelnik *et al* [42] made use of Rundgren's procedure, allowing them to get an excellent agreement between LEED and density functional theory (DFT) results. Finally, Li *et al* [43] reported work where LEED analysis was used for the determination of large molecule adsorption geometries and also used the optimized MT potential approach. They then determined the surface geometry of $C_{60}$ on Ag(111) and demonstrated that a monolayer of $C_{60}$ on Ag(111) induces a substrate reconstruction, producing vacancies that are occupied by $C_{60}$ molecules. However, it seems that the approach leads to real improvement in the structure determination of some systems and has little influence on other systems. Thus *a priori* knowledge of which kind of system it will be more suitable for is not yet clear.

*2.1.2. A full potential for the multiple scattering.* A more accurate LEED structural determination may be achieved by using a full potential to describe the multiple scattering. To obtain a full potential calculation, the classical and straightforward finite difference method (FDM) to solve partial differential equations has been used [44–47]. The FDM consists in transforming the continuous domain of the state variables into a network or mesh of a set of discrete points

and then replacing the derivatives in the differential equations by a set of finite difference approximations involving the neighboring points. In this way, the potential for a crystalline solid can be calculated by dividing the unit cell in a three-dimensional grid, with the Schrödinger equation being solved in a discrete way at each node of the grid. The wavefunctions, exactly the main unknown part of the problem, at the grid points can be obtained by solving a system of linear equations. In the vicinity of the atomic nuclei they are expanded into the usual radial and spherical parts. Following this approach a completely shape-free potential can be calculated in such a way for which there is no constraining to the MT approximation. However, at least up to now, this method has been shown to be unfeasible for practical computer calculations, due to the requirement of high memory and has been shown to be a very time-consuming procedure.

In order to apply this finite differences scheme to LEED calculations, Wu *et al* [29] proposed a new scheme for the application of the FDM to calculate the full potential of the crystal. In this approach, the unit cell is divided into thin slices, parallel to the surface, and the reflection and transmission coefficients of each slice are calculated by replacing the Laplacian in the Schrödinger equation by a fourth-order finite difference for each grid point. Slices with arbitrary thickness are added together, starting from the deepest slice and up to the top one, in order to calculate the total reflection coefficient. This coupling process is similar to the 'layer-doubling' method used in LEED multiple scattering calculations but with two main differences: firstly, in the layer-doubling method pairs of slices of the same thickness are combined, whereas in this proposed method the slices can be of arbitrary thickness and, secondly, in the former, each slice contains at least one layer of atoms while in the latter the slices do not need to have any atoms and so the thickness can be very small. They tested this multi-slice finite difference approach for a Si(111)$(1 \times 1)$ surface and obtained a set of LEED-IV curves in good agreement with the experimental ones [29]. The authors claim that, with today's parallel computers, the use of a full potential of the multiple-slice FDM may become of practical use.

### 2.2. Direct methods

The dynamical nature of the scattering process occurring in LEED prevents a direct extraction of structural information from the experimental data. Although the conventional LEED analysis has been the main approach used to solve the majority of known surface structures, several arbitrary processes in the analysis greatly reduce the reliability of the results, because it is impossible to verify the uniqueness of the structure determination. This drawback places LEED dynamical analysis in disadvantage over a method based on kinematic diffraction, such as surface x-ray diffraction (SXRD), where the crystallographic structure is obtained directly without a prior assumption for the structural model. In this direct method a dependence only on the measured data and an inversion algorithm which is free from assumptions of structural and calculated quantities are expected.

In the crystallography of bulk samples, the so-called direct methods constitute a class of techniques that have been used to recover the phases associated with the measured diffraction intensities. The phases can be used to obtain the complex amplitudes of the scattered waves and the sample structure can be achieved by performing an inverse Fourier transform of these amplitudes. This is the main methodology used in bulk x-ray crystallography. This method has been extended to the case of surfaces and, in order to get more intense scattering, the radiation is incident at glancing angles with respect to the surface. Although this SXRD approach has been showing good results, it has some experimental difficulties, such as the requirement of a synchrotron light source for a good structure determination (for a good review, see [48]). Therefore, surface structure determination by direct methods using techniques other than SXRD is very demanding. Ideally, a direct method starts with measured spectra and inverting them to obtain the atomic geometry, without having to input model-dependent factors such as scattering factor, electron mean free path, thermal vibration amplitudes, etc.

The multiple scattering events occurring in electron diffraction have prevented, for several years, the use of the technique as a direct method. However, after the works of Szoeke [49], Barton [50], Adams and Landman [51] and Chang *et al* [52], two direct methodologies have been developed for electron diffraction. In the first, a Patterson function from LEED-IV spectra is recovered. In the second, which is based on the idea of the optical holography method, the sample atomic positions ($\vec{r}_i$) are obtained by three-dimensional data inversion of the measured intensity fluctuations of electron-diffracted beams. Interference of diffracted waves is present in both methods and a direct inversion scheme is performed, but these two methods are conceptually different. In the holography, the interference between a wave from a reference atom and object waves from nearby atoms is considered. Therefore, the holographic method is intrinsically a multiple scattering process. On the other hand, single scattering processes also occur in the electron diffraction and their interference pattern can, in principle, be inverted to get a Patterson function, similarly to single-energy x-ray diffraction pattern inversion. The problem is how to separate the two contributions from the measured diffraction pattern. Figure 2 shows schematically the two processes, while the bases and performances of the methods applied to LEED are presented in the following sections.

*2.2.1. The Patterson function.* In x-ray crystallography, the experimental data are used by obtaining the Fourier inversion of the diffracted intensities, the so-called Patterson function, which gives the vector positions of every atom relative to every other atom in the unit cell. Therefore, application of this kinematic approach to LEED would make it a more useful technique for surface crystallography. In the case of x-ray diffraction, the Patterson function is the Fourier transform of the diffracted intensities:

$$P(xyz) = \sum_h \sum_k \sum_l I_{hkl} \mathrm{e}^{-2\pi \mathrm{i}(hx+ky+lz)} \qquad (8)$$

where $I_{hkl}$ is the intensity of the $hkl$ reflection. Usually, symmetry can be considered and then, as the intensities of

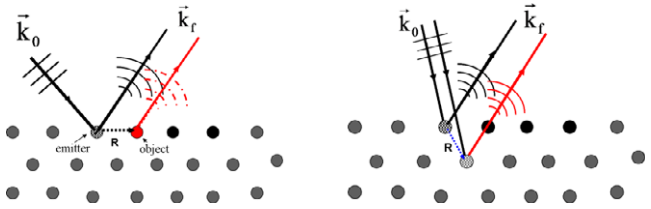


**Figure 2.** Schematic diagrams of the two direct methods. On the right is the holographic diffraction process, and on the left is the Patterson single scattering process.

symmetric beams are equal, $P(xyz)$ turns out to be a real even function. In the case of electron diffraction, the Laue condition along the surface normal is not properly applied and the intensity of an $hk$ beam varies continually along the $l$ direction of the reciprocal space. Thus, the corresponding Patterson function can be written as

$$P(xyz) = \sum_h \sum_k e^{-2\pi i(hx+ky)} \left( \int I_{hk} e^{-iq_\perp z} \, dq_\perp \right) \qquad (9)$$

where $q_\perp$ is a surface normal component of a scattering vector $\vec{q} = \vec{k}_f - \vec{k}_i$. In general, symmetry conditions cannot be applied and $P(xyz)$ is a complex function. The real-space structure is obtained by the convolution square root of $P(xyz)$. In LEED, a two-dimensional periodicity requires that the diffracted beams have a final momenta $\vec{k}_{f\parallel} = \vec{k}_{i\parallel} + \vec{g}_\parallel$, where $\vec{g}_\parallel$ is a two-dimensional reciprocal lattice vector of the sample. Therefore, the Patterson function can be obtained by a phase sum integral over an extensive range of $q$ values of the form

$$P(\vec{R}) = \left| \sum_{\vec{k}_i} \sum_{\vec{g}_\parallel} \int I(\vec{k}_i, \vec{g}_\parallel + q_\perp \hat{e}_z) e^{i\vec{q}\cdot\vec{R}} \, dq_\perp \right|^2 \qquad (10)$$

where $\vec{R}$, in the phase factor $e^{i\vec{q}\cdot\vec{R}}$, is the vector position in real space [53].

The LEED diffracted intensities can be written, in the far-field approximation [54, 55], as

$$I(\vec{k}_i, \vec{k}_f) \propto \left[ f_1 e^{-i\vec{q}\cdot\vec{r}_1} + f_2 e^{-i\vec{q}\cdot\vec{r}_2} + f_1 f_3 e^{-i\vec{k}'\cdot\vec{r}_f} \frac{e^{-ikr_{13}}}{r_{13}} e^{-i\vec{k}'\cdot\vec{r}_3} \right]^2. \qquad (11)$$

This equation (11) represents the contributions to the diffracted intensity from all scattering centers located at positions $\vec{r}_j$ ($j = 1, 2, 3, \ldots$) with respect to an arbitrary origin and $f_i$ is the scattering factor of atom $i$. The single scattering events, at $\vec{r}_1$ and $\vec{r}_2$, are given by the first two terms, respectively. The third term in equation (11) corresponds to the second-order event, with the incident electron first scattering at $\vec{r}_3$, and then at $\vec{r}_1$, with $|\vec{r}_{13}| = |\vec{r}_1 - \vec{r}_3|$. Thus, the cross-term from single scattering events is $I_{1,2}(\vec{k}_i, \vec{k}_f) \propto f_1 f_2 e^{-i\vec{q}\cdot\vec{r}_{12}}$, where $\vec{r}_{12} = \vec{r}_1 - \vec{r}_2$. At $\vec{R} = \vec{r}_{12}$ the phase $e^{-i\vec{q}\cdot\vec{r}_{12}}$ is exactly the conjugate to that of the phase factor $e^{-i\vec{q}\cdot\vec{R}}$ of the integral in equation (10). Therefore, a maximum in the Patterson function is created at $\vec{R} = \vec{r}_{12}$. Hence, the single scattering produces high-intensity spots in the Patterson function which correspond to the vector positions of atomic pairs. For crystalline materials, independent information is provided by $\vec{r}_{ij}$ within the two-dimensional unit cell. Thus, by changing $\vec{R}$, all the relative positions between atoms can be mapped. However, the presence of multiple scattering events introduces modifications on the Patterson function spots and, consequently, the solution is not unique anymore. Then, the main challenge to get the surface structure from direct inversion of the LEED-IV curves is to minimize the dynamical effects.

It is well known that features present in the dynamical LEED-IV curves strongly depend both on the incident angle and on momentum transfer, while the kinematic components mainly depend on the latter. Thus, keeping the momentum transfer constant, it is expected that averaging several LEED-IV curves over different incident angles eliminates the dynamical components. This was first demonstrated by Lagally *et al* [56] for an Ag(111) surface. They measured the diffracted intensities at a constant momentum transfer ($\vec{q}$) for a range of vectors of the incident ($\vec{k}_0$) and scattered ($\vec{k}_f$) beams of a specular reflection. By averaging the LEED-IV curves, for all angles of incidence ($\theta$) and also azimuth ($\phi$), as a function of the momentum transfer, they showed that the interference of the multiple scattering components is, in fact, reduced to a slowly varying background. The authors claim that this procedure allows us to recover very well the kinematic intensities. This approach has been named as constant momentum transfer averaging (CMTA). Later, but following the same idea of measuring LEED-IV curves for several angles of incidence, Adams and Landman [51] tried to recover the structural parameters from experimental LEED intensities via a deconvolution process, i.e. by applying to LEED the Patterson function methodology of x-ray crystallography. They worked with data from the specularly diffracted beams of Cu(100), Ni(100), Al(100) and Al(111) surfaces, measured at several angles of incidence. The results obtained for these simple clean surfaces have led the authors to conclude that the method could have success in future applications to more complex systems. However, they pointed out the difficulties with the problem of the non-uniqueness of the solution for the convolution equation due to data truncation and additional effects resulting from multiple scattering in mixing the variables. In a more conclusive work, Chang *et al* [52] proposed a Patterson-like scheme for direct inversion of the conventional LEED-IV curves. Using the Si(111)(7 × 7) and Si(113)(3 × 2) surfaces as examples, they performed a Patterson inversion for a set of integer-order and fractional-order LEED-IV curves for a normal incidence configuration, using the integral-energy phase-summing method [52]. The result produced high quality 3D atomic images with a resolution better than 0.5 Å of both surface and bulk atoms.

Wu and Tong [55], using Lagally's idea of averaging several LEED-IV curves in order to eliminate multiple scattering effects, proposed the use of multiple-incidence LEED data to get the cancellation of phase shift effects associated with multiple scattering in the Patterson function. They demonstrated that a more accurate Patterson function can be obtained by using a wide sampling of wavenumbers $\vec{k}$ and

directions $\vec{k}_i$. They worked with the Si(111)($\sqrt{3} \times \sqrt{3}$)R30°–Ga system and proved that strong multiple scattering contributions are not eliminated in the transforms of just normal incidence LEED-IV spectra, either from measurement or calculation. However, using calculated off-normal data, the obtained Patterson function is completely artifact-free, that is, every spot corresponds to a specific inter-atomic vector distance. They also observed that the components parallel to the surface are very accurately determined. These results appears very encouraging for obtaining a way of determining surface structures by direct inversion of the LEED spectra.

This methodology has been applied to the study of some systems: GaN(0001)(1 × 1)–Ga surface [57], GaN(0001)($\sqrt{3} \times \sqrt{3}$)-R30°–Ga surface [58, 59], Si(111)(1 × 1)-$YSi_2$ [60] and Si(111)(4 × 1)-In surface [58, 59, 61]. More recently, Kuzushita *et al* [62] used the Patterson function method to compare images calculated from theoretical and experimental LEED-IV curves of an Si(111)(1 × 1)-Fe surface, in order to distinguish between the two proposed models (faulted and unfaulted) for this surface. The authors concluded that, by including several incidence angles, the relative atomic positions in the plane parallel to the surface and in the subsurface of the normal plane were obtained correctly. Also, they observed that a faint peak in the image of the experimental curves does not appear in the image constructed from the unfaulted model, indicating then that the faulted model should be preferable to describe the surface.

In principle, the values of the Patterson function, calculated in a predefined real-space volume, consist of a set of maxima corresponding to the positions of the atomic pairs, the resultant map containing the relative positions of surface atoms. However, in all the works mentioned above, the authors complained about the occurrence of spots that do not come from the structure under study. This fact brings difficulties to the process of assigning spots, with the correct structure not being obtained directly from the experimental LEED data but also by the inversion of the calculated LEED-IV curves for preconceived structural models. The reliability of the values associated with the obtained atomic positions depends then on the accuracy of the experimental data, as well as on the errors introduced by multiple-incidence Patterson inversion. Therefore, residual factors, such as anisotropic vibrations of atoms near the surface, defects or disorder on the surface, may result in a weak noise that can be misinterpreted with real spots. On the other hand, the size of the integration domain in the calculation of the Patterson function is the main factor determining the occurrence of shifts at the spot positions, and the broadening and overlapping of spots. However, it seems that the results so far obtained with the application of the method show that measurements made at low temperatures or recorded on samples as perfect as possible, and also measuring as many beams at different angles for as many energies as possible, would cause the structural surface determination via the Patterson function to be a more accurate process. However, although the method has presented some relative success, only limited progress has been made and it still requires improvements to become a useful procedure. The main advantage of the method is that the analysis, based on the Patterson function, is very fast if compared with the standard LEED procedure. So, although it may be difficult to determine the surface structure correctly by using only the analysis of the Patterson function, it can be useful at least as a supplementary method of conventional LEED analysis. First, by using the Fourier transform of the measured data, a structure that at least is close to the real one can be obtained and then the conventional refinement method can be used.

*2.2.2. The holographic approach.* In optical holography, as originally proposed by Gabor [63], the light, with known amplitude and phase in all directions coming from a point source, illuminates an object. Using a beamsplitter, a diffraction pattern on a detector can be observed far away from the object as a result of the interference between the reference wave ($R$) coming directly from the source and the object scattered wave ($O$) (see figure 2). If the scattering is isotropic, the object's distance from the source can be determined by a Fourier transformation of the measured intensity on a sphere at the far-field. The condition for pattern formation is that the relative phase between $R$ and $O$ is preserved.

To apply these optical ideas to electron diffraction, we have to deal with the problem of defining the reference wave, a challenge that arises from the difficulties in getting sources of coherent electron beams. This problem was first overcome with Szöeke's suggestion [49] that the photoelectrons should be an appropriate source for electron holography because the photoelectrons coming out from a surface are originated from an emitting atom or have first undergone scattering events by the neighboring atoms located at atomic distances away from the emitter. In fact, Barton [50] used the optical analogy to propose that an image of the three-dimensional crystal structure of a solid surface can be created by solving the two-dimensional Kirchhoff–Helmholtz integral to reconstruct a photoelectron diffraction pattern. Later on, this idea was extended to the holographic properties of LEED patterns by considering as a 'splitter', for the incident beam, an adatom on a surface [64–67]. In this approach, the adatom acts as an atomic source of electrons where the backscattered electrons can be seen as the reference waves ($R$) and the forward scattered electrons are scattered again by the nearby atoms (substrate atoms) forming therefore the object waves ($O$) and an interference pattern is generated at the position of the detector. If the adatoms are disorderly distributed on a crystalline surface, a diffused pattern is superimposed on the substrate (discrete) pattern. The two-dimensional diffused LEED pattern (DLEED) can be inverted by a Fourier transform to reconstruct a real-space image of the adsorption site.

By following the optical principle for holography in order to have a hologram [68, 69], the phases of the object wave ($O$) have to be measured and the way to do that is recording the interference between a reference wave ($R$) and the scattered (object) waves, namely

$$A(\vec{k}_i, \vec{k}_f) = R(\vec{k}_i, \vec{k}_f) + O(\vec{k}_i, \vec{k}_f). \tag{12}$$

The intensities of the interference pattern can be obtained by squaring the wavefield amplitudes $A(\vec{k}_i, \vec{k}_f)$:

$$I(\vec{k}_i, \vec{k}_f) = |R(\vec{k}_i, \vec{k}_f) + O(\vec{k}_i, \vec{k}_f)|^2 = |R|^2 + |O|^2 + [RO^* + R^*O]. \tag{13}$$

The second term on the right-hand side of equation (13) contains the interference between the scattered waves and is usually referred to as the classical diffraction pattern. The so-called holographic diffraction pattern comes from the third term (in brackets) in equation (13), because it arises from the superposition of the interference between the unscattered reference wave from the source and the scattered wave from the object. Holographic diffraction dominates the images for small objects, that is, objects that block only a fraction of the cone of radiation arriving at the screen. As the object becomes larger, the reference wave weakens whereas the scattered wave amplitude increases and, when it dominates the image, we are in the classical optical regime described by the diffraction of macroscopic objects. The two cross-terms inside the brackets on the right-hand side of equation (13) generate, under inversion by a Fourier transform, a real and a twin image. Because the reconstruction procedure is phase-sensitive, it not only gives an image at the position of the object, but also at the same distance on the other side of the source.

Equation (13) can be better understood considering the scattering of an atom (emitter) at a position $\vec{r}_a$ on a crystalline surface. Let $A_a(\vec{k})$ be the total amplitude of incident waves on this atom which will generate scattered waves that are rescattered by the atoms in the vicinity of the emitter at position $\vec{r}_a$. The resultant amplitude of these scattered waves, at position $\vec{r}$ relative to $\vec{r}_a$, can be written as [67, 70, 71, 54, 72]

$$A_s(\vec{k}) = \sum_j A_j \frac{f_s(\vec{k}_i, \vec{k}_f)}{r_j} e^{i(kr_j - \vec{k}\cdot\vec{r}_j)} \tag{14}$$

where $A_j$ accounts for the amplitude of the component waves generated by the emitter in the direction of the nearby scattering location ($\vec{r}_j$) and $f_s(\vec{k}_i, \vec{k}_f)$ is the scattering factor of these nearby atoms. Hence, the reference and object waves can be considered respectively as $R(\vec{k}) = A_a(\vec{k})$ and $O(\vec{k}) = A_s(\vec{k})$. Thus, the intensities $I(\vec{k}_i, \vec{k}_f)$ become

$$I(\vec{k}_i, \vec{k}_f) = |A_a(\vec{k})|^2 + |A_s(\vec{k})|^2 + A_a(\vec{k})^* A_s(\vec{k}) + A_a(\vec{k}) A_s(\vec{k})^*. \tag{15}$$

By replacing $A_s(\vec{k})$ in equation (15) as defined in equation (14), the dependence of the intensities of the LEED pattern on the position $\vec{r}_j$ of the atoms in the vicinity of the emitter is explicitly represented.

If we denote the source wave intensity as $I_0(\vec{k}) = |A_a(\vec{k})|^2$, a new function, normalized with respect to $I_0(\vec{k})$, can be defined by

$$\chi(\vec{k}) = \frac{I(\vec{k}_i, \vec{k}_f) - I_0(\vec{k})}{I_0(\vec{k})} = \frac{|A_s(\vec{k})|^2 + A_a(\vec{k})^* A_s(\vec{k}) + A_a(\vec{k}) A_s(\vec{k})^*}{I_0(\vec{k})}. \tag{16}$$

As proposed by Saldin and Chen [71], the measured intensities can be normalized by a function defined as the inverse of the coefficients of the exponential terms in equation (16), with the unknown atom positions $\vec{r}_j$ replaced by a general vector $\vec{r}$:

$$\frac{1}{K(\vec{k}, \vec{r})} = A_a(\vec{k}) A(\vec{r}) \frac{f_s(\vec{k}_i, \vec{k}_f)}{r}. \tag{17}$$

Then, the real-space distribution around the emitter atom (adsorbate) can be recovered from the measured intensities by performing a Fourier transform of equation (16) normalized by the function defined in equation (17), via the following expression:

$$B(\vec{r}) = \int\int K(k_\perp, \vec{k}_\parallel, \vec{r}) \chi(k_\perp, \vec{k}_\parallel) e^{i(kr_j - k_\perp z)} \, dk_\perp e^{i(\vec{k}_\parallel \cdot \vec{r}_\parallel)} \, d^2\vec{k}_\parallel \tag{18}$$

where the Kirchhoff–Helmholtz integral has been divided into two components: one surface integral over $\vec{r}_\parallel$ and one over $\vec{r}_\perp$ perpendicular to the surface. As the data are usually provided on a Cartesian grid ($\vec{r}_\parallel$, $\vec{r}_\perp$), this integration procedure is important when working with ordered superstructures [73].

In fact, the function $K(\vec{k}, \vec{r})$ defined in equation (17) represents some weighting factor for the reference wave and it cancels the coefficients of the exponential when $\vec{r} = \vec{r}_j$, allowing correction for the anisotropy of the reference wave. This results in a good stationary phase condition in the integral over $\vec{k}$, only for the real-space points, enabling a better imaging reconstruction. Besides, it has been shown that the use of such a $\chi$ function has some advantages [54, 73, 71, 74]. It helps to filter out the self-interference terms $|R|^2$ and $|O|^2$ in the DLEED intensity which are responsible for spurious high values of the real-space distribution $|B(\vec{r})|^2$ in the region near the origin. In addition, it helps to suppress modulations in the DLEED patterns that arise from some partial ordering among the emitter (adsorbate) atoms.

Ideally, to obtain a clear image, the Kirchhoff–Helmholtz reconstruction formalism should be used without approximations. However, there are several spurious scattering contributions to the holographic intensities that, if they are not determined in a correct way, the obtained image will be 'noisy', resulting in undesirable deviations of the determined atomic positions. In fact, the main research efforts have been directed towards minimizing such effects. It is expected that the hologram reconstruction procedure will be much easier if the reference wave is as simple as possible, such that the first term on the right-hand side of equation (13) would represent a 'constant' background that can be subtracted easily and if the scattering process generates isotropic object waves on the detector (small variation of $|O(\vec{r})|^2$). In addition, if the reference wave is much stronger than the object wave ($|R(\vec{k})|^2 \gg |O(\vec{r})|^2$), the fourth term in equation (13) does not contribute significantly to the image. Once these conditions are satisfied, a reconstructed image can be obtained using only the cross-terms of equation (13). Of course, the last conditions are unlikely to hold generally. For example, a small object wave amplitude compared to that of the reference wave may occur, depending on the efficiency of the atoms to scatter the incident electrons. For example, in the case of a strong forward scattering, the object wave is originated from an atom deeper in the surface and the term $|O(\vec{r})|^2$ cannot be neglected. In this case, the Fourier transform results in an autocorrelation function instead of a real-space image. On the other hand, the object wave spatial distribution resulting from multiple scattering processes is governed by anisotropy of the scattering factors. Therefore, a serious difficulty is how to deal with the complicated anisotropies and energy

dependence of the reference and object waves. To overcome this difficulty, some attempts have been made on designing a more accurate integration kernel $K(\vec{k},\vec{r})$. For example, Seubert *et al* [75, 76] showed that the 'ghost atoms' appearing on the reconstructed image of the $(2 \times 2)$ phase of 6H-SiC$(000\bar{1})$ were avoided by using a more accurate kernel, based on an iterative procedure. Also, Wu *et al* [77] using experimental data from the system Si(111)R30°$(\sqrt{3} \times \sqrt{3})$–Ga proposed a two-step method to overcome the problem of multiple, nonequivalent reference atoms where a new non-bulk bond kernel is used to point to the reference atom. In addition, there are other problems in performing an image reconstruction from an LEED holographic pattern such as the multiple beamsplitter and twin image formation which may cause serious distortions of the reconstructed image if the distance from the source to the object is of the same order of magnitude as the resolution of the method. A good review about the errors involved in LEED holography reconstruction can be found in [54].

All these proposed approaches have been tested in different surfaces [65, 71, 73, 75, 76, 54, 77, 78] and some advances have been made, but the technique still has problems and more efforts directed toward the methodology are necessary in order to get a more reliable technique, especially for the case of more complex surfaces. Therefore, the decision to apply the methodology of inversion of a holographic LEED pattern has to be taken with great care. However, there is the so-called 'differential holography' proposed by Omori *et al* [79] for the case of photoelectron holography and it seems that it has not been applied to the LEED case yet. The method consists in replacing the normalized hologram $\chi(\vec{k})$ based on intensities measured over the three-dimensional $\vec{k}$ space by its $k$ derivative $\chi'(\vec{k}) = \frac{\partial \chi}{\partial k}$ or by a numerical difference between two $\chi(\vec{k})$'s at different energies, that is $\delta\vec{k} = \chi(\vec{k}+\delta\vec{k}) - \chi(\vec{k})$. More recently, Suzuki *et al* [80] applied this method to a holographic imaging of the $TiO_2(110)$ surface structure. They claim that reduction of the artifacts, twin images and distortions have been successfully achieved and it may be useful for LEED holography. Finally, it must be said that the surface structure determination, via LEED holography, is still not a simple task and it only makes sense if the conventional dynamical LEED calculations represent a more complex procedure.

### *2.3. The tensor LEED approximation*

With the goal of developing an approach to speed up the calculation of the LEED-IV curves, perturbative methods have been conceived, with the so-called tensor LEED method being the most widely used [81–89]. The basic idea of the tensor LEED approximation is as follows. Given a set of LEED-IV curves calculated from an arbitrary 'reference' structure, the changes in the diffracted intensities resulting from small displacements of the atoms away from the reference structure can be evaluated as a perturbation expansion in terms of those displacements.

Let us assume that the atomic positions in the reference structure are described by a set of $\vec{r}_j$ vectors. An incident electron beam with energy $E$ and wavevector parallel to the surface $\vec{k}_\parallel$ can be described as

$$\langle \vec{r}|\vec{k}\rangle = \mathrm{e}^{\mathrm{i}\vec{k}\cdot\vec{r}} \tag{19}$$

where $\vec{k} = (\vec{k}_\parallel, \vec{k}_z)$ and $|\vec{k}_z| = \sqrt{2E - |\vec{k}_\parallel|^2}$ is the wavevector component perpendicular to the surface.

After interacting with the reference structure, the incoming electrons are multiple scattered by the atoms, generating the out-coming LEED states $|\psi^+(\vec{k}_\parallel)\rangle$. The diffracted beams leaving the surface can be written as

$$\langle \vec{r}|\psi^+(\vec{k}_\parallel)\rangle = \sum_g A_g \mathrm{e}^{\mathrm{i}\vec{k}_g\cdot\vec{r}_j} \tag{20}$$

where $\vec{g}$ is a reciprocal lattice vector of the reference structure, $\vec{k}_g = (\vec{k}_\parallel + \vec{g}, \vec{k}_{g,z})$ and $k_{g,z} = \sqrt{2E - |\vec{k}_\parallel + \vec{g}|^2}$.

It is then possible to see that the coefficient $A_g$ is simply the scattering amplitude and then

$$A_g = \sum_j \langle \vec{k}_g|t_j|\vec{k}\rangle$$

where $t_j$ is the scattering matrix associated with atom $j$, with the diffracted intensity being given by

$$I \approx \left|\sum_j \langle \vec{k}_g|t_j|\vec{k}\rangle\right|^2 = |A_g|^2.$$

The scattering matrix $t_j$ is normally evaluated in a standard LEED program.

Another structure, related to the reference structure, can be created by moving the atoms by $\delta\vec{r}_j$ with respect to the corresponding reference positions. The new atomic positions are then defined by $\vec{r}_j + \delta\vec{r}_j$, resulting in a new structure, known as a trial structure. For the reference structure the scattering matrix for atom $j$ is expressed by

$$t_{j,l} = \frac{\mathrm{e}^{2\mathrm{i}\delta_{j;l}} - 1}{2\mathrm{i}k} \tag{21}$$

where $\vec{k}$ is the incident wavevector inside the crystal and $\delta_{j;l}$ is the phase shift associated with the $j$th atom. In the tensor LEED approximation the scattering matrix of the $j$th atom in the trial structure can be given by

$$t''_{j;l} = t_{j;l} + \delta t_{j;l}(\delta\vec{r}_j). \tag{22}$$

After an expansion of $\delta\vec{r}_j$ in an angular momentum basis, it is possible to conclude that $\delta\vec{r}_j$ depends only on the phase shifts and the displacements of the $j$th atom [81–83]. Thus, $\delta\vec{r}_j$ is a geometrical quantity which does not depend on the complex dynamic processes that occur in the reference structure.

For a trial structure not very far from the reference one (small values of $\delta\vec{r}_j$), the scattering amplitude of a diffracted beam is given by

$$A_g^{\mathrm{trial}} = A_g + \delta A_g \tag{23}$$

where, in a first-order approximation,

$$\delta A_g = \sum_j \langle \psi^+(\vec{k}_\parallel + \vec{g}) | \delta t_{j;l} | \psi^+(\vec{k}_\parallel) \rangle \tag{24}$$

where $|\psi^+(\vec{k}_\parallel + \vec{g})\rangle$ are the LEED states from the reference structure excited by an incident beam of parallel wavevector $\vec{k}_\parallel + \vec{g}$.

The intensity of the diffracted beams from the trial structure can be evaluated from

$$I_g \approx |A_g + \delta A_g|^2. \tag{25}$$

The last equation shows that, as $\delta A_g$ depends only on the geometry, the new diffracted intensities can be obtained without the necessity of performing a full dynamical LEED calculation. This allows us to evaluate, in an efficient and fast way, the diffracted intensities from an arbitrary structure similar to the reference structure, thus resulting in a powerful method for LEED analysis. This methodology has been applied in a great number of surface structure determinations [6, 89]. The method has been extended to the problem of exploring the chemical composition and thermal properties, resulting in the so-called chemical and thermal tensor LEED [85, 86, 88].

### *2.4. The nanoLEED approach*

With the boom in nanoscience and nanotechnology, knowledge of the detailed atomic structure of low dimensionality systems such as nanoparticles, carbon nanotubes and nanowires is a real necessity in order to better understand their unique physical, chemical and biological properties. However, many of the relevant systems for technological applications may not present a well-defined periodicity. As already pointed out, standard LEED relies on long-range order to determine the atomic geometry of surfaces and interfaces. The long-range order requirement precludes the use of traditional LEED in crystallographic studies of nanoscale aperiodic systems. Grazing incidence small-angle x-ray scattering (GISAXS) has already been used with some degree of success to gain information about the shape and size distribution of metal nanoclusters supported on oxide surfaces, but with little detail about defects or bond length and bond angles between atoms [90]. Scanning tunneling microscopy (STM) has also been used to probe the structure of low dimensionality systems, but STM results rely heavily on theoretical simulations that are not always straightforward to perform [91].

In principle, reducing the lateral dimension of the electron incident beam to the nanometer scale would allow to focus the incident beam into a small region containing a single (or a few) nanostructure. The coherent length of the incident beam must be smaller than the nanoparticle size in order to reduce contributions from defects and borders. As in the calculations only elastically scattered electrons are considered, improved energy filters must be used in the experiment. The diffracted beams leaving the nanostructure could then be used to probe the geometric structure of the nanostructure itself. Experimentally, this could be achieved by using an STM tip as an electron source [92] or using a convergent electron beam as has already been proposed and dubbed convergent-beam LEED (CBLEED) [93]. By comparing the experimental and theoretical diffracted beam intensities, the structure of the nanomaterial can, in principle, be solved. However, several modifications must be done in the standard LEED theory to perform LEED diffracted intensity curve simulations for a single nanostructure.

Recently, the standard LEED theory was adapted to a cluster approach where diffracted intensity curves can be evaluated from ordered and disordered nanosystems [94–97]. In this approach, named nanoLEED, the cluster includes all of those atoms of the nanoparticle that contributes for the electron elastic scattering. Exit-direction-dependent diffracted intensities by the whole cluster are calculated and compared with the experimental data for ordered systems.

To evaluate the diffracted intensities it is necessary first to calculate the scattering matrices $T_i$ containing all the scattering events inside the cluster ending at atom $i$ by solving the matrix–vector equation:

$$t = (I - tG)T = CT \tag{26}$$

where $t$ is a block-diagonal matrix composed of the atomic scattering $t_i$ matrices for individual atoms, $C$ is the complete scattering matrix of the cluster, $G$ is the free-electron propagator function between two atoms and $I$ is the identity matrix. Since the computational effort of inverting the $C$ matrix scales with $N^3$ or $N^2$, where $N$ is proportional to the number of atoms in the cluster, the inversion method becomes prohibitive in the cluster methodology and new approximated methods must be used. In the nanoLEED approach, the total scattering matrix $C$ is split into three parts by grouping the atoms according to their relative distances:

$$C = C_{d<d_{\mathrm{CG}}} + C_{d_{\mathrm{CG}}<d<d_{\mathrm{UV}}} + C_{d>d_{\mathrm{UV}}}. \tag{27}$$

For each distance range, a most efficient iterative method for solving the multiple scattering problem is applied. The first term in equation (27) contains only atoms closer than a $d_{\mathrm{CG}}$ distance from one another and the (bi)conjugate gradient method (BiCG) [98] is used to evaluate the scattering $C_{d<d_{CG}}$ matrix. In LEED we have to solve a matrix–vector equation of the type $Ax = b$. Since usually $A$ is non-Hermitian, the BiCG method considers both the matrix–vector equation $Ax = b$ and its adjoint matrix–vector equation $x^*A^* = b^*$. The BiCG method generates, at each step, the approximate solution, the corresponding residuals, the search directions that will be used in the next step and the two orthogonal sequences that are simultaneously minimized. If the residual norm satisfies a predefined stopping criterion, the algorithm stops and the approximate solution is considered close enough to the real solution. The efficiency of the BiCG method is determined by the condition number of a matrix defined as $\kappa(C_{d<d_{\mathrm{CG}}}) = \|C^{-1}_{d<d_{\mathrm{CG}}}\| * \|C_{d<d_{\mathrm{CG}}}\|$. For a low condition number, a reliable and fast convergence is usually obtained. In practical calculations, a $d_{\mathrm{CG}}$ value of about 0.2 nm has proven to be adequate [95].

The second term in equation (27) contains only pairs of atoms with intermediate separations in the range $d_{\mathrm{CG}} < d <$

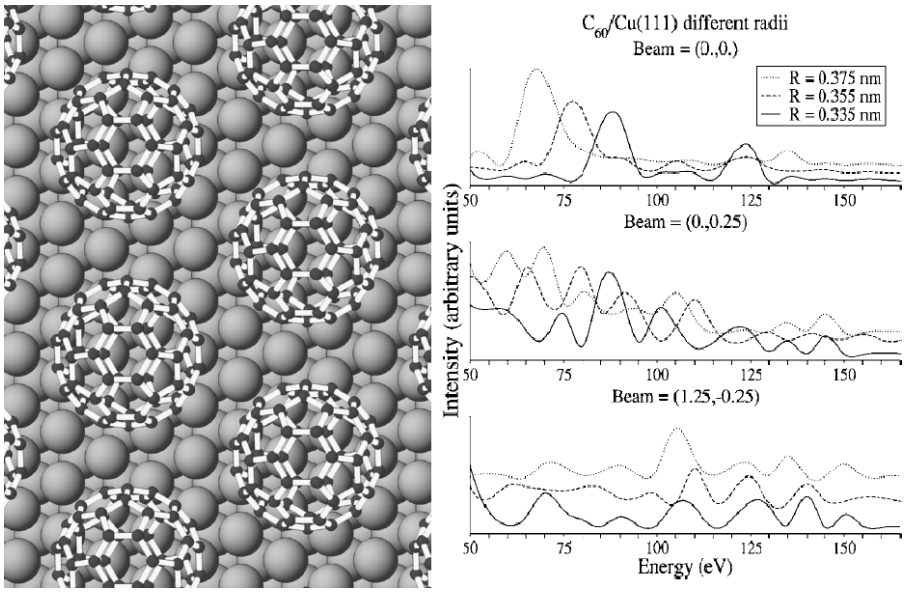


**Figure 3.** NanoLEED simulations of LEED-IV curves for Cu(111)(4 × 4)-$C_{60}$ for different molecule radii demonstrating the structural sensibility of the nanoLEED approach. Reproduced with permission from [94] (right) and [95] (left). Copyright 2006 and 2007 by the American Physical Society.

$d_{UV}$, where $d$ is the separation between two atoms and $d_{UV}$ is a system-dependent cutoff distance, above which the UV method becomes inefficient. In this intermediate region the scattering matrix rank $r$ (the number of columns and rows that are linearly independent) becomes nearly constant and has lower values and a singular value decomposition method is more suitable than the UV methodology. In the singular value decomposition method, an $N \times N$ matrix can be split into a product of a matrix $U$ with $N \times r$ and a matrix $V$ with $r \times N$ [99]. Due to the low value of the matrix rank, the UV method performs better than the standard conjugated gradient method.

The sparse matrix canonical grid (SMCG) method [100] is most effective in LEED when dealing with a large number of atoms and large inter-atomic distances. For this reason, the last term in equation (27) contains pairs of atoms that are relatively distant from each other and the SMCG method is used to solve the multiple scattering problem. First, a rectangular grid is generated even if a random cluster is used. Then, each atom of the cluster is assigned to its closest grid point and the electron wave propagating from atom $i$ to atom $j$ is forced to pass through the grid points nearest to the two atoms. The scattering between the two grid points is efficiently calculated by the SMCG method and, finally, the grid-related scattering matrix is shifted back to the real atomic positions.

NanoLEED calculations were performed for ordered and disordered nanosystems demonstrate the sensibility of the diffracted intensities to changes in the nanostructure. For Cu(111)(4 × 4)–$C_{60}$, the simulations have shown that by changing the $C_{60}$ radius by 5%, corresponding to a change of 0.075 Å in the C–C distances, produces considerable shifts on the peak positions of the LEED-IV curves (figure 3). These shifts are the signature of high structural sensitivity. The same structural sensitivity was observed in nanoLEED simulations of the electron diffraction patterns and energy/angular-dependent diffraction curves on silicon nanowires [96].

## 3. The conventional LEED analysis: searching for an *R*-factor global minimum

Since the first days of LEED structural surface determination, several optimization methods have been used to identify the reliability factor minimum. This step of the LEED structural analysis is strictly numerical and it is not related to the methods for electron scattering calculations.

An exhaustive search for coincidence between two sets of points representing two curves is a search process that belongs to the class of an NP-complete optimization problem. This usually requires a large computational effort to locate the solution which is not bounded by a polynomial in $N$. This special class of problems is of great importance in the theory of numerical analysis, but it remains a problem of difficult solution despite the great advances in computational capability.

In practical terms the search procedures have an efficiency that is case-dependent. Thus, the scaling behavior obtained for a specific problem does not necessarily match the solution of similar problems.

The search methods used in LEED can be roughly classified in two broad sets: (i) methods based on trial-and-error search and (ii) methods based on some systematic route for minimization of the cost function, i.e. the reliability factor ($R$ factor). The first structural determinations by LEED involved a trial-and-error process [7, 10] with the values for the parameters being assumed from a blend of indirect hints and guesses in the process of trying to fit experimental and theoretical curves. The parameters are correlated in such a way that, when adjusting one parameter, this implies a readjustment of the others. This was a strong limitation, restricting application of LEED to simple structures, which prompted the quest to find a more systematic route for the adjustment process, i.e. an automated search. The first structural

determination using an automated process was performed by Powell and de Carvalho [101]. In that work, a variation of the steepest descent method was used, i.e. the partial derivatives of the $R$ factor with respect to the $N$ parameters were used as a guide in the search for the minimum of the cost function.

A few months before the work by Powell and de Carvalho, a theoretical work by Rous *et al* [81] was published reporting the tensor LEED approach. This method, while not being strictly a search method, is useful for structure refinement with adjustment of structural parameters on a scale of a fraction of an ångström.

Afterward, several approaches, sometimes a combination of methods, have been used for LEED structural determinations: tensor LEED with gradient methods [81, 89], the so-called direct methods using approaches similar to the ones adopted in x-ray crystallography [11, 102, 103] and methods using the least-squares procedures [104]. Each of these methods have their own deficiencies, either by being too time-consuming for computational calculation or by being unable to distinguish between local and global minima. Frequently, a combination of optimization methods is used, with one method exploring a wider area of the parameter space, followed by another for a refinement in an area close to a previously identified possible minimum. To avoid the possibility of identifying a local minimum as a global one, Rous [105] applied the method of the simulated annealing (SA) algorithm to the search problem in LEED. His results, based on a theory–theory comparison, present, for dependence of the computational cost with the number of explored parameters, a scaling relation given by $N^6$, with $N$ being the number of parameters. Motivated by this first attempt of establishing a global search method to the LEED problem, Nascimento *et al* [106, 107] investigated an alternative approach to the SA, the so-called fast simulated annealing (FSA) approach [108]. In this method, the adopted random step distribution function is a Cauchy–Lorentz function, instead of a Gaussian (or uniform) one, as employed in the SA approach. This modification has proved to be extremely useful, since the scaling factor becomes linear with the number of parameters $N^1$ at least for the systems for which the procedure was tested.

Another approach for identifying the global minima in the LEED search process was proposed by Kottcke and Heinz [109], which includes an optimization of the theory–experiment fitting process using a random sampling algorithm. In contrast to the SA or FSA approaches, the random sampling algorithm only takes into account downhill moves, with a multiple launching process (several starting structures), thus being a compromise between global and local search methods. This procedure turns out to have an $N^{2.5}$ scaling with the number of parameters.

Blanco-Rey and de Andres [110], following the random sampling algorithm idea, proposed a search method, called combinatorial simultaneous optimization (SO), which works on two levels. In the first level, good candidate structures are determined using a simplified dataset chosen at random inside the experimental database. Each element of the chosen dataset yields one nonlinear equation, thus resulting in a system of nonlinear equations that can be solved and the process is repeated for different chosen datasets. In the second level, the nature of the minimum (whether local or global) is tested by selecting structures with a Gaussian distribution and therefore allowing uphill moves. However, despite having nearly 100% success rate, the method showed a not-so-good scaling ($N^{4.1}$) for an Ir(110)-p(2 × 1) missing-row surface theory–theory comparison.

Motivated by the relative success of the SA algorithm, as employed by Rous [105], which requires a high number of structures to be tested, Döll and Van Hove [111] proposed applying to the LEED structural determination process another global search algorithm, called the genetic algorithm (GA) [7, 112]. This is a method that mimics the natural evolution of living organisms. Recently, some effort has been done in testing, more systematically, the GA approach to the LEED structural determination [113, 114]. The GA methodology has proved to be a powerful tool for LEED search, when used simultaneously with local search methods, such as the Powell and simplex methods [113] and it exhibits a favorable scaling behavior of $N^{1.5}$.

Recently an approach that simultaneously increases the radius of convergence (as compared with the tensor LEED) and includes a global search for a minimum of the $R$ factor was proposed [115]. This new method uses a new approximation for the tensor calculation, termed frozen LEED (FL), with the important advantage of increasing the radius of convergence to over 0.8 Å, while the tensor LEED is normally less than 0.4 Å. Of course, as previously pointed out, this procedure is not a proper search method. However, unequivocally, it scans new possible structures in the vicinity of a reference point in the parameter space (a phase-space point). An SA algorithm is also incorporated in the FL approximation, so that it becomes possible to avoid the chance of ending in a local minima, which is a deficiency of the tensor LEED.

Another approach to the search process in LEED was recently published by Zhao *et al* [116]. In searching for a global optimizer methodology, those authors adapted and developed a pattern search method know as GPS (generalized pattern search), and obtained results that had a better performance than the genetic algorithm, while keeping the necessary robustness of a search method.

### *3.1. Approaches based on simulated annealing*

The SA algorithm is a mathematical model based on a process commonly employed in metallurgy, by which molten metals are systematically and gradually cooled and annealed. If the temperature is reduced at a sufficiently low rate, the atoms will line themselves up, reaching an organized distribution, associated with a crystalline state that depends on specific physical conditions, including the cooling rate. The final state corresponds to the global minimum of the thermodynamical energy associated with the specific physical conditions prevailing during the cooling process. The mechanism of the SA method employs an artificial 'temperature' as a source of stochasticity, thus creating an artificial dynamics that prevents the search process, associated with the minimization of the cost function, from getting trapped in a local minima. After

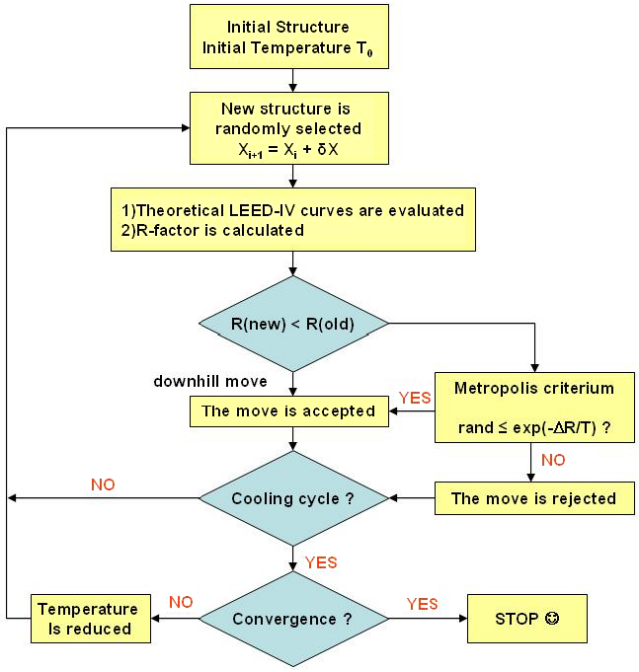


**Figure 4.** Flowchart of the SA algorithm implementation for the LEED structure search.

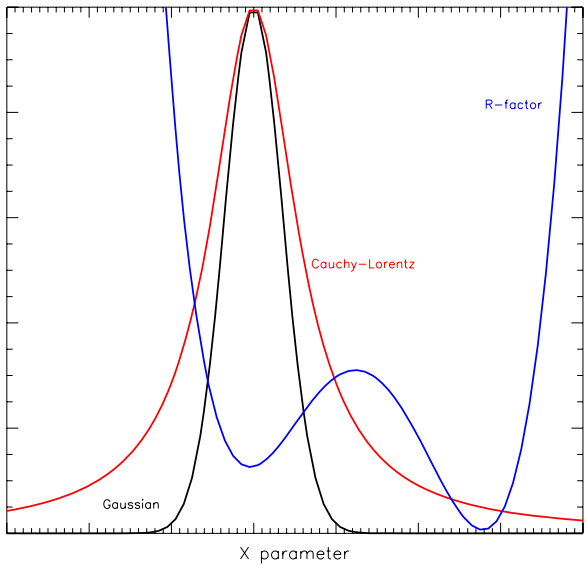


**Figure 5.** Comparison between Cauchy–Lorentz and Gaussian distribution sampling at the same 'temperature'.

several steps of the search process, the 'temperature' is very low and hopefully the optimization process results in obtaining a set of parameters such that the cost function is located inside the basin of the global minimum. In this situation the search steps behave asymptotically as a gradient descent local search method. At the core of the SA method is the Metropolis criterion [117] that controls the probability for a step being accepted or not, during the search process. From a certain point in the parameter space, $\vec{X}_i$, a new one is generated by the addition of a random increment, namely $\vec{X_{i+1}} = \vec{X}_i + \delta\vec{X}$. If the change in the cost function (or energy) is negative or null ($\Delta C = C(\vec{X_{i+1}}) - C(\vec{X}_i) \leqslant 0$) the movement is accepted. However, if $\Delta C > 0$, the movement may be accepted according to a probability given by a Boltzmann distribution, i.e. if $P(\Delta C) = \mathrm{e}^{-\frac{\Delta C}{T}}$ is greater than or equal to a random number between 0 and 1. This probability is controlled by the artificial 'temperature' parameter, which is gradually reduced during the search process.

The first implementation of SA for LEED was performed by Rous [105] using the Van Hove–Tong conventional LEED code [10]. The basis of the structure of the search process is illustrated in figure 4. The method was applied to locate the global minimum for a Pendry $R$-factor ($R_\mathrm{P}$) [118] hypersurface generated by a theory–theory comparison for the Ir(110)(2 × 1) surface. A scaling relation was obtained that is able to characterize how the number of structures explored before convergence is related to the number of structural parameters. This method has shown a dependence of $N^{6.0}$. In this first implementation for LEED, the random steps were randomly chosen according to a uniform distribution, which was not dependent on the 'temperature' parameter.

The main problem associated with the SA is that its convergence is slow. Thus, to improve the efficiency of the SA, one needs to figure out how to improve the cooling of the search process, turning it as fast as possible and, simultaneously, avoiding an increase in the probability of the search process to get trapped in a local minimum.

The most common approach, called classical SA, also known as a Boltzmann machine [119], uses a Gaussian distribution as a way to generate the random steps taken during the search process. A Boltzmann–Gibbs acceptance probability is then employed. In adopting the Boltzmann machine, the cooling scheme is such that the temperature decreases logarithmically with time along the search steps [120].

Szu and Hartley [108] proposed an SA search machine that uses a Cauchy–Lorentz distribution for the generation of the random steps. This semi-local distribution, in contrast to the Gaussian distribution, allows the occurrence of occasional long steps. These long steps improve the probability of convergence and allow a faster cooling scheme (see figure 5). A Boltzmann–Gibbs acceptance probability is also adopted and a faster cooling scheme is employed: the temperature decreases with the inverse of time. This approach is known as FSA or a Cauchy machine.

A generalization of both annealing schemes was then proposed [121] based on the non-extensive Tsallis statistics [122–124], which was able to provide annealing schemes even faster than the FSA one. This non-extensive statistics is based on the generalization of the Boltzmann–Gibbs entropy [125], being now employed in a wide variety of fields [126, 127].

The desirable features for a global search method in LEED are: (1) a high probability of locating the global minimum for the $R$ factor among all other local minima and (2) a favorable scaling relation with respect to the number of parameters to be varied during the search process. In the first SA implementation for LEED [105], as previously discussed, an unfavorable scaling relation was

obtained ($N^6$), despite its success in locating the global minimum. Motivated by the initial work of Rous [105] and with the goal of obtaining a more favorable scaling, Nascimento *et al* [106, 107] decided to investigate the possible implementation of the FSA method to the search problem in LEED, using the conventional Van Hove–Tong LEED code [10]. The results obtained indicate the FSA algorithm as a promising option for global optimization in LEED, since the scaling factor becomes linear with the number of parameters ($N^1$). This conclusion results from the application of the FSA approach in a CdTe(110) theory–theory comparison. Another good point is that the probability of convergence, as a function of the number of parameters, presented a slowly decreasing behavior. The FSA algorithm was also applied to real structural determinations, in theory–experiment comparisons, for the Ag(111), Ag(110) and CdTe(110) systems [106, 107, 128] showing the same behavior as that of theory–theory comparison.

More recently, Correia *et al* [129] implemented the generalized simulated annealing (GSA) approach for the LEED problem, along the lines of the non-extensive statistical mechanics [121–123]. A generalized distribution function was adopted, according to the value associated with a parameter $q_V$ [129]. Several different distribution functions (random steps) and cooling schemes have been used in investigating their influence on the performance of the GSA when applied to the LEED search problem. Again, the algorithm was applied to a theory–theory comparison for the CdTe(110) system, but now for a normal incident geometry (in contrast to an off-normal geometry in the previous work [107]). The results indicate that, among the several values tested for the $q_V$ parameter within the GSA approach, the FSA scheme was the best one due to the favorable linear scaling ($N^1$) and the slowly decreasing probability convergence with the number of structural parameters being optimized.

### *3.2. The genetic algorithm*

GAs are gradient-free and parallel global optimization algorithms. They use a performance criterion (fitness) for evaluation and work with a population of possible solutions in the search for a global minimum among several other local minima. GAs are capable of handling complex and irregular solutions in multidimensional spaces. They have been applied to a wide range of difficult optimization problems, from container loading optimization and learning robot behavior to game theory [130]. In condensed matter physics, it has been applied to optimize geometric structures [131–134], tight-binding parameters [135] and shaping cluster expansion Hamiltonians [136]. GAs are particularly useful in search processes where the parameters are strongly correlated, cases where other optimization methods can lead to a local minimum, instead of a global one.

The GAs are a class of evolutionary algorithms inspired by the biological Darwinian theory, mimicking the natural evolution of living organisms through the process of natural selection, using the 'survival-of-the-fittest' model from nature. Good solutions are selected and manipulated to achieve new, and possibly better, solutions. In the GA terminology, an individual represents a set of parameters which, in principle, is a candidate solution. The selection process is based on the fitness of the individual, which is evaluated through a function, not necessarily algebraically expressed, that defines the problem. To perform the manipulation process, the individuals must be encoded in strings, like 'chromosomes'. There are several ways by which the individuals can be encoded, such as a binary or a real encode. For all kinds of codifications there are manipulation devices that are able to exchange information between individuals, giving rise to new ones. The individuals are combined in a searching process that maximizes the fitness, either by minimizing or maximizing a 'cost function' [112]. The initial population is randomly chosen and then individuals taken from different positions of the solution space can have their 'genes' mixed by genetic sequential operator devices, such as crossover, elitism and mutation [137].

**Table 1.** Example of the binary (a) and the real (b) encode representations used in the GA implementation in LEED.

| (a) | | | (b) | | |
|---|---|---|---|---|---|
| $x_1$ | $x_2$ | $x_3$ | $x_1$ | $x_2$ | $x_3$ |
| 0101001011 | 1011001000 | 1000111010 | 0.85 | 0.72 | −0.15 |

The GA has, with respect to other global search methods, the advantage of having 'memory' from the past, as well as the possibility of 'learning', as a route for improving characteristics considered as adequate, while discarding others assumed or considered as being inadequate under a previously established criterion.

The codification of typical parameters, characteristics of the LEED search process, is performed using a binary or real representation by associating their values to the chromosomes, which together form a string. In the realm of the GA, a string represents an idea while each bit (its intrinsic value and position on the string) is related to a notion.

The initial population consists of a certain number of individuals, each one randomly generated within a set of predetermined physical limits, according to physical considerations. In a binary codification, the strings consist of a series of bits, where each part of the string represents an $x_i$ parameter to be optimized in the search process. For example, in the case of three parameters, each parameter can be codified by 10 bits resulting in a string of 30 bits, as illustrated in table 1(a). If a real codification is used, the strings consist of a series of real numbers, where each number corresponds to an $x_i$ parameter to be optimized, as represented in table 1(b).

After generating the initial population, the strings are tested, according to the LEED code, with the respective $R$ factors being used to calculate probabilities of selection for the evolutionary devices. Once the individuals are encoded and their fitness evaluated, the population is ready to be submitted to the process of crossover, elitism and mutation in order to give rise to a new generation. The process is successively repeated, with each step having characteristics as described in the following. The GA directs the process towards the best region in the parameter space by crossover and elitism. In the

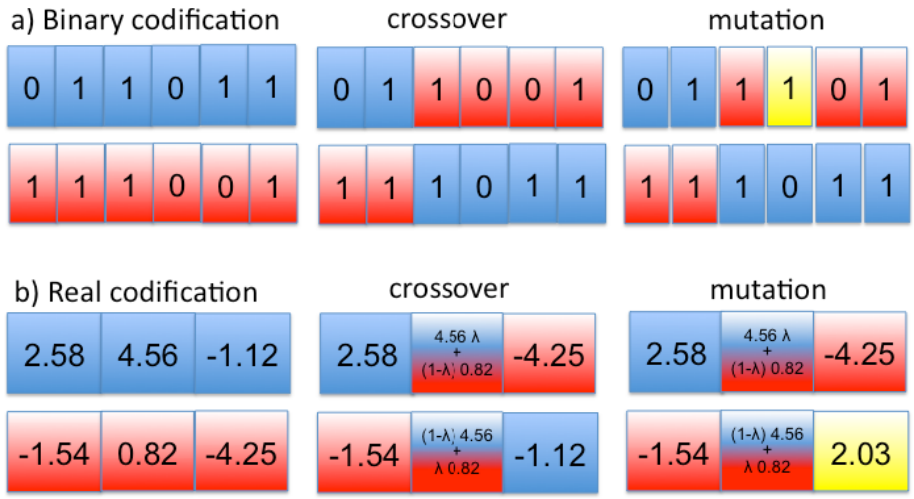


**Figure 6.** Examples of crossover and mutation schemes in GAs for binary (a) and real (b) codification. (a) A pair of individuals blue (dark gray) and red (gray) (parents) are mixed by the crossover operation, generating new individuals that will belong to the next generation. (b) In the real codification, new individuals are created by initially selecting the parameters that will be modified, keeping the others only for exchange, and then randomly choosing the λ coefficient that is used to generate the offspring parameters by a linear combination of the parent's parameters. Yellow (light gray) bits represent bits that were modified by mutation.

crossover, portions of the strings resulting from the previous step are mixed together, giving a chance to create new strings with different characteristics. The members of the population to undergo the crossover are randomly chosen in pairs (obeying a precalculated probability of selection) with the cut position being also randomly chosen, followed by a permutation of the parts. Alternatively, the members of the population with higher fitness can have a corresponding higher probability of being chosen to participate in the crossover. As illustrated in figure 6(a), for a pair of individuals blue (dark gray) and red (gray) (parents) in a binary representation, with cut position between the second and third bit, the crossover mixes the chromosomes of parents to generate individuals of the next generation. The new individuals have inherited characteristics from parents as illustrated by the blue–red and red–blue individuals. To illustrate the crossover in the real codification, there is shown in figure 6(b) one kind of crossover, where new individuals are created as follows: the parameters that will be modified are initially selected, keeping the others only for exchange, as exemplified in the binary crossover. In the following, the λ coefficient is randomly chosen and used to generate the offspring parameters by a linear combination of the parents' parameters.

In the context of the GA, elitism refers to the process of transferring to the next generation the best-fit individuals of the preceding generation. In the paper by Döll and Van Hove [111], this step was applied considering that 'it turns out that the convergence speed is increased by applying elitism, whereby the best chromosome of the preceding population enters the next one in any case'. Thus, those authors selected the 10% individuals judged by their fitness as the most suited for further generations, and directly transferred them to the following generation. Thus, a possibility that can be considered on implementing elitism is to do this before crossover, i.e. to transfer to the next generation the $X\%$ individuals with best fitness. After that, the crossover is implemented among all individuals of the previous generation, transferring to the next generation the $(100 - X)\%$ best suited (for a fixed size of the population). Another approach for applying elitism is to implement it after crossover. In doing so, recombination, as described in the previous step, is performed for all individuals, leaving the competition to occur between parents and descendants, according to the respective fitness, transferring to the next generation the ones most fitted (keeping the population size constant). This change on the criterion for fitness affects the convergence speed [114].

The following step is mutation. This step allows the exploration of regions of the parameter space previously not contained in the strings, by randomly changing values of the bits. The mutation rate should not be too high, since that would cause the loss of information contained in the original population, and neither too low, otherwise nothing new would be brought into the population.

In the example presented in figure 6, the mutation in the binary representation consists in the change of a 0 to a 1 (or vice versa) at one or more positions of the string (yellow (light gray)). In the real representation, the mutation operator randomly changes the value of the selected parameter as illustrated in figure 6(b). This step of the process allows the appearance of 'new notions' and this does not occur in any other step, since elitism and crossover just copy or recombine pre-existent notions already available in a previous generation.

A schematic flowchart of the GA algorithm implementation for LEED structure determination is presented in figure 7. Initially, a population of $N$ individuals is generated. Each individual is a vector containing the $P$ parameters to be optimized in the structural analysis of the system. The value of each parameter is randomly chosen within a physically acceptable range for that system. Each individual is coded as a binary or real string that will contain the displacements

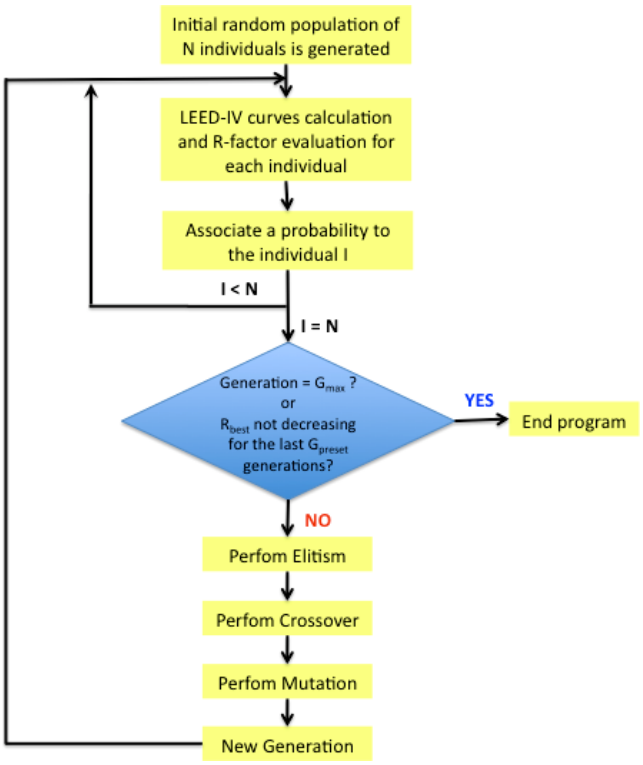


**Figure 7.** Flowchart of the GA algorithm implementation for the LEED structure search.

to be added to the parameters of a reference initial surface structure. The LEED-IV theoretical curves are then evaluated for each individual $I \leqslant N$, and the comparison with the experimental curves is carried out returning the $R$ factor value associated with each individual $I$. Based on its $R$-factor value, the probability of being selected for crossover is calculated for individual $I$. That probability should give rise to individuals with lower $R$ factors having higher chances to be selected for the crossover process, without completely excluding the worst ones. The search stops here if the best $R$ factor has not decreased after a preset number of generations or if a preset maximum number of generations is reached. Then the best individual in the last generation is selected as the best solution. Otherwise, the best individual is cloned to the next generation (by elitism) and the process continues. As in other optimization methods, the stopping criterion changes from case to case. If the stopping criterion is not achieved, $N/2$ pairs of individuals are chosen according to probabilities based on their $R$ factors. The crossover process then creates $N$ new individuals for the next generation. The worst one is discarded, being replaced by the clone obtained by elitism. A number between 0 and 1 is chosen randomly. If this number is smaller than a previously chosen mutation rate, then a randomly chosen individual is subjected to the mutation process. The new generation is now ready, and the process restarts for the new generation.

The GA implementation, as described above, was applied to surface structural determination by LEED of three previously solved systems: Ni(111)($\sqrt{3} \times \sqrt{3}$)-R30°–Sn, InSb(110) and CdTe(110) and proved to be a very helpful tool [138]. The structures found as the best ones in each case are in close agreement with those previously published. The scaling behavior analysis suggests a scaling factor of around 1.3, based on a theory–theory comparison for the CdTe(110) system. This scaling factor is very competitive when compared to previously applied methods.

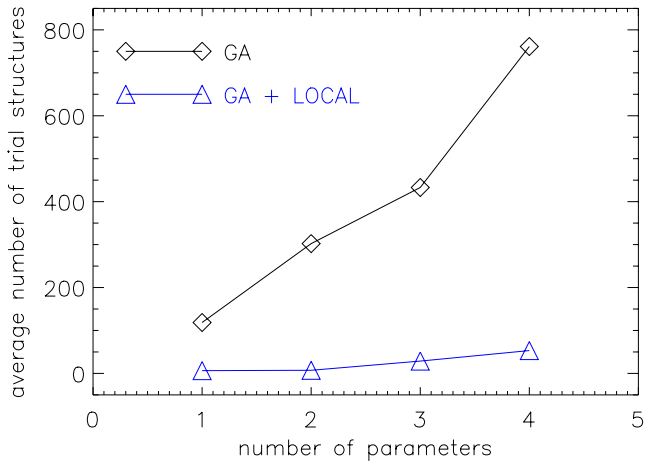


**Figure 8.** Scaling behavior for the standard GA and for the GA with simultaneous local refinement applied to the Ni(111)($\sqrt{3} \times \sqrt{3}$)-R30°–Sn system.

What it is really expected from a global optimization method such as the GA is to identify the 'basin' in which the global minimum is located. Once inside this, conventional local optimization methods like steepest descent are much more efficient to find the optimum. One could have the benefit from both methods by devising a hybrid approach in which we alternate the global search capability of a GA and the efficiency of a local optimization method. Viana *et al* [138] have thus implemented a scheme by which each new trial structure generated by GA is first locally optimized before it is used in the next GA step of recombination (crossover). Figure 8 shows the scaling behavior for the standard GA, and for the GA with simultaneous local refinement applied to the Ni(111)($\sqrt{3} \times \sqrt{3}$)-R30°–Sn system. As can be seen, at least for this system, the search was much faster (speeded up by more than an order of magnitude) using the local refinement simultaneously with the global search of the GA algorithm.

## 4. Final remarks

Detailed knowledge of the geometric structure of surfaces in nanoscaled systems, including bond lengths and angles, is essential for a complete understanding of their unique physical and chemical properties. However, this is not a simple task. There exist a few techniques that can be used for this proposal, with all of them having been successful only for relatively simple systems. The most widely used of these techniques is LEED. For long-range ordered surfaces and interfaces LEED has undoubtedly demonstrated its capability of quantitatively probing the structural properties. It is the technique that has

been used in the great majority of structural investigations up to now. However, this technique still has difficulties in revealing the structure of more complex surfaces, where a large number of atoms has to be considered. In the last decade, LEED has undergone some advances and the main objective of this review was to illustrate the present status of the technique and to demonstrate the considerable improvements that became possible by recent methodological developments, mostly on the theoretical and data analysis aspects.

The fascinating application possibilities of nanosystems are a new source of motivation for the study of nanoscaled systems and the complete understanding of their physical, chemical and biological properties requires a detailed knowledge of the geometric structure of nanoparticles. This is a very exciting research field which makes it worth the hard work of applying LEED to surface structure determination of this class of systems. The recent development of the nanoLEED approach has extended the LEED domains to individual nanostructures, such as nanowires and nanotubes. However, the lack of experimental data, due to technical problems in focusing an electron beam within a region of a few square nanometers, is, at least for a while, precluding the use of LEED in the crystallographic studies of isolated nanostructures and more effort must be made to develop appropriate electron beam sources.

In the standard structural LEED determination, an *R*-factor methodology has been intensively applied. In this methodology, the search for the best structural model is equivalent to a minimization problem, having the *R* factor as the cost function to be minimized. However, due to the dimension and complexity of the space of parameters to be investigated, the application of this methodology is, in general, a very time-consuming task. Local minima in the hyperspace can result in trapping the solution and actions must be taken to overcome this problem. The use of global optimization methods in the search process seems to be a promising way to speed up the LEED structure determination. Some of these approaches have been used in LEED analysis, each one showing advantages as well as limitations. All applied methods have shown an improvement in the probability of escaping from local minima and therefore have speeded up the search process significantly.

A better description of the scattering potential seen by the electrons has led to some improvements in the structure determination by LEED, especially for those systems with marked directional bonds, such as metal oxides and semiconductors. Improvements in the electron scattering description may play a key role in the future of the structural determination of more complex systems.

The electron diffraction structure determination by direct methods, namely Patterson function and LEED holography, are much faster than the conventional LEED calculations, which is certainly an advantage. However, several problems related to experimental data collection have to be solved before this methodology can be routinely applied. In fact, the use of a direct method must, at least, be helpful when using it for generating a more probable structure that may be used as a starting point for the LEED analysis.

Finally, the development of novel materials and processes, with both technological and scientific interest, requires knowledge of the surface and interface properties at the atomic scale. Thus, the main challenge for LEED is to be improved to solve the structure of new complex systems.

## Acknowledgments

The authors would like to acknowledge the Brazilian science agencies (FAPEMIG, FAPESB and CNPq) for financial support.

## References

[1] Elsasser W 1925 *Naturwissenschaften* **13** 11
[2] Davisson C J and Kunsman C H 1923 *Phys. Rev.* **22** 242
[3] Davisson C J and Germer L H 1927 *Nature* **119** 558
[4] Davisson C J and Germer L H 1927 *Phys. Rev.* **30** 705
[5] Wood E A 1963 *J. Appl. Phys.* **35** 1306
[6] Heinz K 1995 *Rep. Prog. Phys.* **58** 637
[7] Van Hove M A 1997 *Surf. Rev. Lett.* **4** 479
[8] Van Hove M A 2009 *Surf. Sci.* **603** 1301
[9] Van Hove M A, Weinberg W H and Chani C-M 1986 *Low Energy Electron Diffraction—Experiment, Theory and Surface Structure Determination* (Berlin: Springer)
[10] Van Hove M A and Tong S Y 1979 *Surface Crystallography by LEED* (Berlin: Springer)
[11] Pendry J B 1974 *Low Energy Electron Diffraction* (London: Academic)
[12] Lipson H and Cochran W 1965 *The Determination of Crystal Structures* (Ithaca, NY: Cornell University Press)
[13] Adams D L 2002 *Surf. Sci.* **519** 157
[14] Surface Science Group 2009 http://www-jenkins.ch.cam.ac.uk/techniques/index_leed.html
[15] Lindsay R, Wander A, Ersnt A, Montanari B, Thornton G and Harrison N M 2004 http://www.phantomsnet.net/files/abstracts/ECSCD8/Orals_LindsayR.pdf
[16] Soares E A, Leatherman G S, Diehl R D and Van Hove M A 2000 *Surf. Sci.* **468** 129
[17] Ferralis N, Li H I, Hanna K J, Stevens J, Shin H, Pan F M and Diehl R D 2007 *J. Phys.: Condens. Matter* **19** 056011
[18] Dorel S, Pesty F and Garoche P 2000 *Surf. Sci.* **446** 294–300
[19] Pesty F and Garoche P 2003 *J. Appl. Phys.* **94** 7910
[20] Heinz K and Muller K 1982 *Structural Studies of Surfaces* (*Springer Tracts in Modern Physics* vol 91) pp 1–53
[21] de Carvalho V E, Cook M W, Cowell P G, Heavens O S, Prutton M and Teat S P 1984 *Vacuum* **34** 893
[22] Mattheiss L F 1964 *Phys. Rev.* **133** A1399
[23] Loucks T L 1967 *Augmented Plane Wave Method* (New York: Benjamin)
[24] Schattke W 2000 *Prog. Surf. Sci.* **64** 89
[25] Hatada K, Hayakawa K, Chaboy J and Natoli C R 2009 *J. Phys.: Conf. Ser.* **190** 012010
[26] Baranov A N, Stepanyuk V S, Hergert W, Katsnelson A A, Settels A, Zeller R and Dederichs P H 2002 *Phys. Rev.* B **66** 155117
[27] Kheifets A S, Lun D R and Savrasov S Yu 1999 *J. Phys.: Condens. Matter* **11** 6779
[28] Rundgren J 2003 *Phys. Rev.* B **68** 125405
[29] Wu H, Wang J, So R and Tong S Y 2007 *J. Phys.: Condens. Matter* **19** 386203
[30] Nascimento V B, Moore R G, Rundgren J, Zhang J, Cai L, Jin R, Mandrus D G and Plummer E W 2007 *Phys. Rev.* B **75** 035408

[31] Rundgren J 1999 *Phys. Rev.* B **59** 5106
[32] Zabloudil J, Hammerling R, Szunyogh L and Weinberger P 2006 *Phys. Rev.* B **73** 115410
[33] Hedin L and Lundquist B I 1971 *J. Phys. C: Solid State Phys.* **4** 2064
[34] Walter S, Blum V, Hammer L, Müller S, Heinz K and Giesen M 2000 *Surf. Sci.* **458** 155
[35] Moritz W 2000 *Manual of the LEEDFIT Code*
[36] Pentcheva R, Wendler F, Meyerheim H L, Moritz W, Jedrecy N and Scheffler M 2005 *Phys. Rev. Lett.* **94** 126101
[37] Pentcheva R, Moritz W, Rundgren J, Frank S, Schrupp D and Scheffler M 2008 *Surf. Sci.* **602** 1299
[38] Lübbe M and Moritz W 2009 *J. Phys.: Condens. Matter* **21** 134010
[39] Mulakaluri N, Pentcheva R, Wieland M, Moritz W and Scheffler M 2009 *Phys. Rev. Lett.* **103** 176102
[40] Derry G N, Wan R, Krueger E, Waldt J and English C 2009 *Surf. Sci.* **603** 2193
[41] Meyer W, Biedermann K, Gubo M, Hammer L and Heinz K 2008 *J. Phys.: Condens. Matter* **20** 265011
[42] Kostelnik P, Seriani N, Kresse G, Mikkelsen A, Lundgren E, Blum V, Sikola T, Varga P and Schmid M 2007 *Surf. Sci.* **601** 1574
[43] Li H I *et al* 2009 *Phys. Rev. Lett.* **103** 056101
[44] Seitsonen A P, Puska M J and Ieminen R M 1995 *Phys. Rev.* B **51** 14057
[45] Benham S P, Thijssen J M and Inglesfeld J E 2000 *Comput. Mater. Sci.* **17** 160
[46] Joly Y 2001 *Phys. Rev.* B **63** 125120
[47] Mayer A 2006 *Phys. Rev.* E **74** 046708
[48] Saldin D K and Shneerson V L 2008 *J. Phys.: Condens. Matter* **20** 304208
[49] Szöeke A 1986 *Short Wavelength Coherent Radiation: Generation and Applications* (*AIP Conference Proceedings* vol 147) ed D T Attwood and J Boker (New York: American Institute of Physics)
[50] Barton J J 1988 *Phys. Rev. Lett.* **61** 1345
[51] Adams D L and Landman U 1977 *Phys. Rev.* B **15** 3775
[52] Chang C Y, Lin Z C, Chou Y C and Wei C M 1999 *Phys. Rev. Lett.* **83** 2580
[53] Wu H and Tong S Y 2001 *Phys. Rev. Lett.* **87** 036101
[54] Tong S Y 1999 *Adv. Phys.* **48** 135
[55] Tong S Y and Wu H 2002 *J. Phys.: Condens. Matter* **14** 1231
[56] Lagally M G, Ngoc T C and Webb M B 1971 *Phys. Rev. Lett.* **26** 1557
[57] Xu S H, Wu H S, Dai X Q, Lau W P, Zheng L X, Xie M H and Tong S Y 2003 *Phys. Rev.* B **67** 125409
[58] Wang J, Wu H, So R, Liu Y, Xie M H and Tong S Y 2005 *Phys. Rev.* B **72** 245324
[59] Wang J, So R, Liu Y, Wu H, Xie M H and Tong S Y 2006 *Surf. Sci.* **600** L169
[60] Rogero C, Martin-Gago J-A and de Andres P L 2003 *Phys. Rev.* B **67** 073402
[61] Abukawa T, Yamazaki T and Kono S 2006 *Surf. Sci. Nanotechnol.* **4** 661
[62] Kuzushita T, Murata A, Yamamoto A and Urano A 2008 *Appl. Surf. Sci.* **254** 7824
[63] Gabor D 1948 *Nature* **161** 777
[64] Saldin D K and de Andres P L 1990 *Phys. Rev. Lett.* **64** 1270
[65] Saldin D K, Harp G R, Chen B L and Tonner B P 1991 *Phys. Rev.* B **44** 2480
[66] Mendez M A, Glück C and Heinz K 1992 *J. Phys.: Condens. Matter* **4** 999
[67] Starke U, Pendry J P and Heinz K 1996 *Prog. Surf. Sci.* **52** 53
[68] Xu W, Jericho M H, Meinertzhagen I A and Kreuzer H J 2002 *Appl. Opt.* **41** 5367
[69] Midgley P A and Dunin-borkowski R E 2009 *Nature Mater.* **8** 271
[70] de Andres P L 1991 *Phys. Scr.* **T39** 318
[71] Saldin D K and Chen X 1995 *Phys. Rev.* B **52** 2941
[72] Heinz K, Starke U and Bernhardt J 2000 *Prog. Surf. Sci.* **64** 163
[73] Reuter K, Schardt J, Bernhardt J, Wedler H, Starke U and Heinz K 1998 *Phys. Rev.* B **58** 10806
[74] Wei C M and Tong S Y 1992 *Surf. Sci.* **274** L577
[75] Seubert A, Saldin D K, Bernhardt J, Starke U and Heinz K 2000 *J. Phys.: Condens. Matter* **12** 5527
[76] Seubert A and Heinz K 2002 *Surf. Rev. Lett.* **9** 1413
[77] Wu H, Xu S, Ma S, Lau W P, Xie M H and Tong S Y 2002 *Phys. Rev. Lett.* **89** 216101
[78] Kolthoff D, Schwennicke C and Pfnür H 2003 *Surf. Sci.* **529** 443
[79] Omori S, Nihei Y, Rotenberg E, Denlinger J D, Kevan S D, Tonner B P, Van Hove M A and Fadley C S 2002 *Phys. Rev. Lett.* **88** 55504
[80] Suzuki A, Hashimoto A, Nojima M, Owaria M and Niheib Y 2008 *Surf. Interface Anal.* **40** 1627
[81] Rous P J, Pendry J B, Saldin D K, Heinz K, Müller K and Bickel N 1986 *Phys. Rev. Lett.* **57** 2951
[82] Rous P J and Pendry J B 1989 *Comput. Phys. Commun.* **54** 137
[83] Rous P J and Pendry J B 1989 *Comput. Phys. Commun.* **54** 157
[84] Blum V and Heinz K 2001 *Comput. Phys. Commun.* **134** 392
[85] Heinz K, Kottcke M, Löffler U and Döll R 1996 *Surf. Sci.* **357/358** 1
[86] Löffler U, Muschiol U, Bayer P, Heinz K, Fritzsche V and Pendry J B 1995 *Surf. Sci.* **331–333** 1435
[87] Rubner O, Kottcke M and Heinz K 1995 *Surf. Sci.* **340** 172
[88] Löffler U, Döll R, Heinz K and Pendry J B 1994 *Surf. Sci.* **301** 346
[89] Van Hove M A, Moritz W, Over H, Rous J P, Wander A, Barbieri A, Materer N, Starke U and Somorjai G A 1993 *Surf. Sci. Rep.* **19** 191
[90] Renaud G, Lazzari R and Leroy F 2009 *Surf. Sci. Rep.* **64** 255
[91] Wen M, An B, Fukuyama S and Yokogawa K 2009 *Surf. Sci.* **603** 216
[92] Mizuno S, Rahman F and Iwanaga M 2006 *Japan. J. Appl. Phys.* 2 **45** L178
[93] Spence J C H, Poon H C and Saldin D K 2004 *Microsc. Microanal.* **10** 128
[94] Gavaza G M, Yu Z X, Tsang L, Chan C H, Tong S T and Van Hove M A 2006 *Phys. Rev. Lett.* **97** 055505
[95] Gavaza G M, Yu Z X, Tsang L, Chan C H, Tong S T and Van Hove M A 2007 *Phys. Rev.* B **75** 014114
[96] Gavaza G M, Yu Z X, Tsang L, Chan C H, Tong S T and Van Hove M A 2007 *Phys. Rev.* B **75** 235403
[97] Gavaza G M, Yu Z X, Tsang L, Van Hove M A and Tong S T 2008 *J. Phys.: Condens. Matter* **20** 304202
[98] Barret R, Berry M, Chan T F, Demmel J, Doanto J, Dongarra J, Eijkhout V, Pozo R, Romine C and Van der Vorst H 1994 *Templates for the Solution of Linear Systems: Building Blocks for Iterative Methods* 2nd edn, vol 1 (Philadelphia, PA: SIAM) chapter 2.3.5, p 21
[99] Tsang L and Li Q 2004 *Microwav. Opt. Technol. Lett.* **41** 354
[100] Barret R, Berry M, Chan T F, Demmel J, Doanto J, Dongarra J, Eijkhout V, Pozo R, Romine C and Van der Vorst H 1994 *Templates for the Solution of Linear Systems: Building Blocks for Iterative Methods* 2nd edn, vol 1 (Philadelphia, PA: SIAM) chapter 2.3.1, p 14
[101] Powell P G and de Carvalho V E 1987 *Surf. Sci.* **187** 175
[102] Pendry J B and Heinz K 1990 *Surf. Sci.* **230** 137

[103] Kleinle G, Moritz W, Adams D L and Ertl G 1989 *Surf. Sci.* **219** L637
[104] Kleinle G, Moritz W and Ertl G 1990 *Surf. Sci.* **238** 119
[105] Rous P J 1993 *Surf. Sci.* **296** 358
[106] Nascimento V B, de Carvalho V E, de Castilho C M C, Costa B V and Soares E A 2001 *Surf. Sci.* **487** 15
[107] Nascimento V B, de Carvalho V E, de Castilho C M C, Soares E A, Bittencourt C and Woodruff D P 1999 *Surf. Rev. Lett.* **5** 651
[108] Szu H and Hartley R 1987 *Phys. Lett.* A **122** 157
[109] Kottcke M and Heinz K 1997 *Surf. Sci.* **376** 352
[110] Blanco-Rey M, de Andres P, Held G and King D A 2004 *Comput. Phys. Commun.* **161** 151
[111] Döll R and Van Hove M A 1996 *Surf. Sci.* **355** L393
[112] Goldberg D E 1989 *Genetic Algorithms in Search Optimization and Machine Learning* (Reading, MA: Addisson-Wesley)
[113] Alvarenga M L V 2004 *Master Thesis* Universidade Federal de Minas Gerais Brazil
[114] de Castilho C M C, de Souza H C S, Santos L A S, Cerqueira M E and Nascimento V B 2005 private communication
[115] Yu Z X and Tong S Y 2005 *Phys. Rev.* B **71** 161404
[116] Zhao Z, Meza J C and Van Hove M A 2006 *J. Phys.: Condens. Matter* **18** 8693
[117] Metropolis N, Rosenbluth A, Rosenbluth M, Teller A and Teller E 1953 *J. Chem. Phys.* **21** 1087
[118] Pendry J B 1993 *Surf. Sci. Rep.* **19** 87
[119] Kirkpatrick S, Gellat C D and Vecchi M P 1983 *Science* **220** 671
[120] Geman S and Geman D 1984 *IEEE Trans. Pattern Anal. Mach. Intell.* **6** 721
[121] Tsallis C and Stariolo D A 1987 *Physica* A **233** 395
[122] Tsallis C 1988 *J. Stat. Phys.* **52** 479
[123] Curado E M F and Tsallis C 1991 *J. Phys. A: Math. Gen.* **24** L69
[124] Tsallis C 1995 *Phys. Lett.* A **206** 389
[125] Boon J P and Tsallis C 2005 *Europhys. News* **36** 185
[126] Tsallis C, Gell-Mann M and Sato Y 2005 *Europhys. News* **36** 186
[127] Tsallis C 2009 *Introduction to Nonextensive Statistical Mechanics: Approaching a Complex World* (New York: Springer)
[128] Nascimento V B, Soares E A, de Carvalho V E, Lopes E L, Paniago R and de Castilho C M C 2003 *Phys. Rev.* B **68** 245408
[129] Correia E d R, Nascimento V B, de Castilho C M C, Soares E A and de Carvalho V E 2005 *J. Phys.: Condens. Matter* **17** 1
[130] http://en.wikipedia.org/wiki/Genetic-algorithm
[131] Deaven D M and Ho K M 1995 *Phys. Rev. Lett.* **75** 288
[132] Ho K M, Shvartzburg A, Pan B C, Lu Z Y, Wang C Z, Wacker J, Fye J and Jarrold M 1998 *Nature* **392** 582
[133] Johannesson G H, Bligaard T, Ruban A V, Skriver H L, Jacobsen K W and Norskov J K 2002 *Phys. Rev. Lett.* **88** 255506
[134] Stucke D P and Crespi V H 2002 *Nano Lett.* **3** 1183
[135] Klimeck G and Bowen R C 2000 *Superlatt. Microstruct.* **27** 77
[136] Blum V, Hart G L W, Walorski M J and Zunger A 2005 *Phys. Rev.* B **72** 165113
[137] Schmitt L M 2001 *Theor. Comput. Sci.* **259** 1
[138] Viana M L, Simões e Silva W, Soares E A, de Carvalho E A, de Castilho C M C and Van Hove M A 2008 *Surf. Sci.* **602** 3395